THE JOURNAL
OF
CHEMICAL PHYSICS

VOLUME 13, NUMBER 2 FEBRUARY, 1945

Hydrogen Overvoltage in Concentrated Sulfuric and Phosphoric Acid Solutions*

ANDRÉ J. DE BÉTHUNE AND GEORGE E. KIMBALL
Department of Chemistry, Columbia University, New York, New York

(Received December 4, 1944)

The overvoltage for the discharge of hydrogen on a mercury cathode has been measured at 25°C in sulfuric acid solutions in the concentration range 0.125 to 9.65 molar. In dilute solution, the overvoltage is independent of the acid concentration, the cathode reaction being the discharge of a proton from water. At concentrations in excess of 2.83 molar, the overvoltage decreases approximately as a linear function of the weight percentage. Evidence is presented to show that in this region, the cathode reaction involves the hydrogen sulfate molecule, H_2SO_4. Preliminary results on phosphoric acid solutions also show a drop in the overvoltage as the concentration is increased beyond 1 molar.

INTRODUCTION

THE current density of discharge of positive ions at a cathode is given by the theory of absolute reaction rates by an equation of the form

$$I=\frac{\epsilon kT}{h}\exp\left[\frac{\Delta S^{\ddagger}}{k}-\frac{\Delta H^{\ddagger}}{kT}-\frac{\epsilon\alpha V}{kT}\right][A^{+}], \quad (1)$$

when the process is activation controlled.[1] $\Delta S^{\ddagger}$ and $\Delta H^{\ddagger}$ are the entropy and heat of activation (per ion), respectively, for the discharge process, $[A^{+}]$ is the activity of the ions in a layer of adsorbed ions adjacent to the cathode, ϵ is the charge on a proton, k Boltzmann's constant, T the absolute temperature, and h Planck's constant. V is the electrical potential between the adsorbed ion layer and its electrical image in the electrode; its sign is defined by the relation:

$$V=V\text{ (metal)}-V\text{ (solution)}. \quad (2)$$

α is the fraction of this double-layer potential operating between the adsorbed ion layer and the top of the potential energy barrier. It is convenient to define the cathodic overvoltage η as:

$$V=V_{eq}-\eta, \quad (3)$$

where V_{eq} is the double-layer potential at an electrode at equilibrium in the given solution with respect to the given electrode reaction.

At hydrogen cathodes in moderately acid and neutral solutions ($0<p\text{H}<7$), the experimentally observed current densities can be represented as a function of the overvoltage by an equation of the form:

$$I=I_0 10^{\eta/b}=I_0\exp\left[\frac{2.3\eta}{b}\right]. \text{ (Tafel's equation).} \quad (4)$$

Bowden[2] showed that, between 0° and 72°C, the factor b does have the temperature dependence predicted by Eq. (1), *viz.*:

$$b=\frac{2.3kT}{\alpha\epsilon}=\frac{59.1mv}{\alpha}\text{ (at 25°C)}, \quad (5)$$

* Publication assisted by the Ernest Kempton Adams Fund for Physical Research of Columbia University.

[1] G. E. Kimball, J. Chem. Phys. **8**, 199 (1940).

[2] F. P. Bowden, Proc. Roy. Soc. **A126**, 107 (1929).

with $\alpha=\frac{1}{2}$ on most metals. This value of α was confirmed by numerous workers. The factor I_0 is very dependent on the metal used, depends on the temperature with energies of activation of the order of 10 to 20 kcal.mole^{-1},[3] is proportional to the $\frac{1}{4}$th power of the hydrogen pressure at pressures not too far below 1 atmosphere,[4] and is independent of the pH of the solution.[5]

The theoretical interpretation of these facts has been given by Eyring, Glasstone, and Laidler,[6] and Kimball, Glasstone, and Glassner,[7] who showed that Eq. (1) can be made to fit the facts if it is assumed that (1) the source of the protons discharged at the cathode is water, (2) that the electrical double layer as it extends outward from the electrode into the solution includes at least two layers of adsorbed ions, so that a proton crossing the double layer must pass over at least two energy barriers before it reaches the electrode. KGG showed that the charge density in the inner ion layer increases with $[H^+]$, p_{H_2}, and η, but that at reasonably high values of these variables, it becomes essentially "saturated," and then shields the inner half of the double layer from any further electrostatic disturbances in the outer half, and vice versa. That part of the reversible potential which varies with the pH of the solution is set up across the outer half of the double layer, while that part which varies with hydrogen pressure operates across the inner half. If the slow step is the passage of a proton across the inner energy barrier, then the overvoltage is also set up across the inner half of the double layer. Thus if the total potential be written as the sum of an inner and an outer potential term:*

$$V=V_i+V_o, \tag{6}$$

where

$$V_i=\frac{-kT}{2\epsilon}\ln p_{H_2}-\eta, \tag{7}$$

and

$$V_o=\frac{kT}{\epsilon}\ln (H^+), \tag{8}$$

only the potential αV_i is operative in activating the discharge reaction. From Eq. (1), the current density should be given by:

$$I=\text{const.}\exp\left[\frac{-\epsilon\alpha V_i}{kT}\right]$$
$$=\text{const.}\ p_{H_2}{}^{\alpha/2}\exp\left[\frac{\epsilon\alpha\eta}{kT}\right], \tag{9}$$

in agreement with experiment when $\alpha=\frac{1}{2}$.

The assumption that the protons come from water molecules accounts for the constancy of the factor $[A^+]$ in Eq. (1) when the pH is varied. The slow step, as postulated by EGL, is the transfer of a proton from a water molecule in the inner ion layer to a water molecule adsorbed on the negatively charged electrode, with the consequent formation of an adsorbed H atom on the cathode, and the liberation of an hydroxyl ion HO^- in the inner ion layer. Since the potential energy barrier exists between two layers of water molecules, it should be symmetrical satisfying the requirement that $\alpha=\frac{1}{2}$.

The heat of activation $\Delta H^\ddagger$ depends largely on the metal used. The higher the energy level of an H atom adsorbed on the metal (one of the products of the postulated slow-step), the higher $\Delta H^\ddagger$, and the greater the overvoltage for a given current density. Metals that are good adsorbents of hydrogen are known to be "low overvoltage" metals, and those that adsorb it poorly are "high overvoltage" metals. By using the values of $\Delta H^\ddagger$ as determined experimentally (from the temperature variation of I at η constant, or of η at I constant),[3] EGL showed that $\Delta S^\ddagger$ is a constant independent of the metal or solution whose value is in fair agreement with the value calculated for the postulated mechanism.

However, if water ceases to be the principal component of the solution, as is the case when one goes to acid solutions of higher and higher concentrations, the overvoltage $\eta(I)$ should no longer be independent of the nature of the

---

[3] Review by F. P. Bowden and J. N. Agar, Ann. Reports Chem. Soc. **35**, 90 (1938).

[4] S. J. Bircher and W. D. Harkins, J. Am. Chem. Soc. **45**, 2890 (1923). M. Knobel, J. Am. Chem. Soc. **46**, 2751 (1924).

[5] F. P. Bowden, Trans. Faraday Soc. **24**, 473 (1928).

[6] H. Eyring, S. Glasstone, and K. J. Laidler, J. Chem. Phys. **7**, 1053 (1939), hereinafter referred to as EGL.

[7] G. E. Kimball, S. Glasstone, and A. Glassner, J. Chem. Phys. **9**, 91 (1941), hereinafter referred to as KGG.

* The standard reversible potentials V_i^0 and V_o^0 are purposely omitted from these equations, since for the purposes of Eq. (1), they are essentially constants which can be incorporated into the heat of activation $\Delta H^\ddagger$.

solution, and should be expected to drop as water is progressively replaced by a stronger acid, i.e., by a better source of protons. This was actually found to be the case with both sulfuric and phosphoric acids, although the overvoltage curves $\eta(I)$ obtained by going to stronger acids were markedly different in the two cases.

EXPERIMENTAL

The cell used and the wiring diagram are sketched in Fig. 1. The cell was made of Pyrex glass and consisted of three compartments, for the anode *A*, the cathode *C*, and the reference electrode *E*, respectively. The cathode and anode compartments were connected by an ungreased

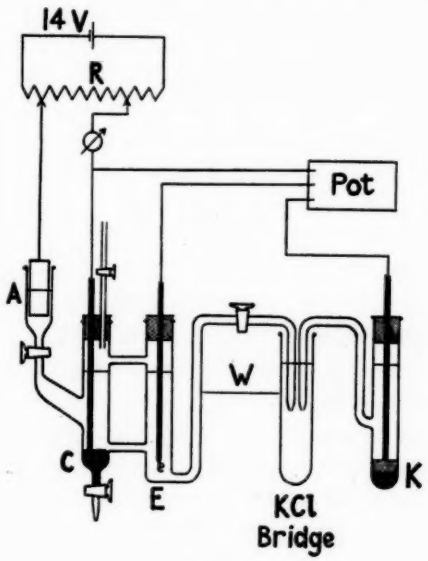

FIG. 1.

stopcock wetted with the solution being electrolyzed. This stopcock was normally kept shut to prevent admission of oxygen into the cathode compartment. The resistance of the system was such that currents up to about 1 ma could be obtained from the seven two-volt batteries in series (except with the most dilute solution employed). By opening the stopcock, currents up to about 10 ma could be obtained. However, after opening and closing the stopcock, a marked depression in the overvoltage $\eta(I)$ amounting to as much as 100 mv could be observed. This was followed by a slow and gradual return of the overvoltage to its steady value before opening the stopcock.

The cell was equipped with two side-arms indicated in Fig. 2. One of these led from a mercury funnel *H* through a lightly greased stopcock into the bottom of the cathode compartment. The other one led into the bottom of the reference electrode compartment and was used to fill the cell with solution.

The reference electrode consisted of a platinized platinum wire sealed into a soft glass tube and held in place by a rubber stopper which had been previously boiled in acid and alkali. The platinum electrode was saturated with hydrogen by being made cathodic *in situ*, and then continued to function as a hydrogen electrode as long as the solution remained saturated with hydrogen. Its potential was controlled against that of a saturated calomel electrode *K*, and remained constant within better than 5 mv in the great majority of the runs.

Electrical contact with the mercury cathode was made through a platinum wire sealed in soft glass, and held in place by a boiled rubber stopper. In this stopper was also inserted a stopcock which led (through a safety trap and a water bubbler not shown in the diagram) to the atmosphere and through which any excess pressure in the cell could be relieved. The area of the cathode was measured by running water out of the cathode compartment (with the platinum wire tube in place) and weighing the amount of water corresponding to a vertical distance of 1 cm. The area was found to be 2.52 ± 0.05 cm^2 ($\log_{10} A = 0.401\pm0.009$).

The sulfuric acid solutions were prepared by dilution of 18*M* product (Baker and Adamson C.P. grade) with distilled water. Before each run, the cell was cleaned with concentrated nitric acid, sulfuric acid$-K_2Cr_2O_7$ solution, distilled water, and then steamed out. The platinum anode and the two platinum wire tubes were then inserted in place, and the stopcocks (ungreased) in the H_2SO_4 train of Fig. 2 were moistened with some of the solution to be electrolyzed. The stopcock at the bottom of the cathode compartment was greased rather thoroughly. The sulfuric acid solution, having been prepared to the approximate strength desired, was brought to the boiling point, and then inserted in the apparatus at *F* (Fig. 2). The pressure over the sulfuric acid was reduced by

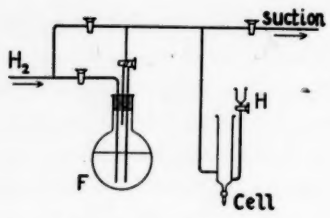

FIG. 2.

suction from a water aspirator, and the liquid allowed to boil under reduced pressure for about 10 minutes to remove the air present. The suction was then cut off and hydrogen (electrolytic tank hydrogen, purified over red hot copper and through NaOH solution and soda-lime) cautiously allowed to bubble into the solution until the pressure had built up again. The hydrogen was then allowed to continue bubbling through the solution and into the electrolytic cell to displace the air present. When the liquid was cooled down, a portion of the solution was forced into the cell to rinse it, and discarded. A second portion of the liquid was then forced into the cell, hydrogen allowed to bubble through it for a few minutes longer, and then shut off. The platinum reference electrode was made cathodic for a few minutes to saturate it with hydrogen. The electrolysis was started between the platinum wire in the cathode compartment and the platinum anode. Redistilled mercury was quickly run into the bottom of the cathode compartment up to the level of the side arm leading to the reference electrode, and the overvoltage determined as a function of the current which could be varied by adjustment of the rheostat R of Fig. 1.

In view of the depolarizing action of oxygen on hydrogen cathodes, the precautions recommended by all workers in this field for the stringent removal of oxygen cannot be too strongly emphasized. In the present series of experiments, the overvoltage $\eta(I)$ generally rose during the first few hours of the run, gradually reaching a maximum and steady value. This indicated the presence of last traces of oxygen in the solution which were gradually removed by reduction at the cathode. This same type of behavior could be reproduced (as noted before) by opening the anode stopcock for a few minutes. The bubbling of "purified" tank hydrogen through the solution led to very unsteady overvoltage values. After reaching a steady value, the overvoltage at any given current $\eta(I)$ remained constant within a range generally not exceeding 20 mv during a period of several days in which the measurements were taken.

The overvoltage was taken as the potential difference between the platinum reference electrode and the mercury cathode:

$$\eta = V_{Pt(H_2)} - V_{Hg}, \qquad (10)$$

as measured by means of a Leeds and Northrup student potentiometer No. 152168, whose smallest scale division is 1 mv. The ammeters used were two multi-range ammeters incorporated in radio-testing-boxes: Model 862 and Model 852 of the Precision Apparatus Company, Brooklyn, New York. In the region of interest, the former of these had scales of 0–12 ma and 0–1.2 ma divided into 60 parts, and the latter had scales of 0–1 ma, 0–100 μa, and 0–50 μa divided into 50 parts. These instruments were used without calibration. They agreed with each other.

In the majority of the runs, the apparatus was immersed up to line W (Fig. 1) in a water thermostat maintained at 25.00±0.03°C. However, for some of the solutions, the measurements were repeated with the cell immersed in air at room temperatures of 24 to 28°C. No difference could be found between the two types of runs, since the effect of this temperature variation is smaller than the experimental uncertainty in the absolute value of the overvoltage.

The concentration of the sulfuric acid was determined by titration with standard alkali on samples of the solution removed from the flask and from the cell both at the start and at the close of a run. The pH was determined from the potential of the platinum reference electrode with respect to calomel, and also from that of a glass electrode with respect to calomel (Beckman pH meter). The procedure used on the three runs with phosphoric acid reported herein differs in no wise from that described above for sulfuric acid.

RESULTS—SULFURIC ACID SOLUTIONS

The overvoltage measurements obtained on eight sulfuric acid solutions, with concentrations

TABLE I. Overvoltage measurements in sulfuric acid at 25°C.

Molarity	Weight %	Potential calomel to hydrogen mv	pH	Potential glass to calomel mv	pH	b mv	α	log I_0 (I_0 in amp./cm²)	Range of measurements log I
0.125	1.2	291.7±0.7	0.96	400.5	0.92	116	0.51	−10.40	−6.40 to −4.15
0.465±0.005	4.4	260.1±0.3	0.42	430.7	0.41	118	0.50	−10.30±0.12	−5.75 to −3.00
2.35 ±0.01	20.2	213.2±1.1	−0.37			116	0.51	−10.43±0.10	−5.00 to −4.25
						130	0.45	− 9.80±0.20	−4.25 to −3.50
2.83 ±0.02	23.7	208.7±0.3	−0.45	485.9	−0.52	115	0.515	−10.58±0.08	−6.00 to −4.25
						147	0.40	− 9.18±0.10	−4.25 to −3.00
4.16 ±0.03	32.8	191.9±0.3	−0.73	500.7	−0.77	117	0.505	− 9.95±0.05	−6.00 to −3.00
5.85 ±0.1	43.3	185.3±0.3	−0.84	523.7	−1.16	83	0.71	−11.70	−6.40 to −5.25
						88	0.67	−11.34	−5.25 to −4.50
						97	0.61	−10.72	−4.25 to −3.50
						116	0.51	− 9.53	−3.50 to −3.00
8.2 ±0.1	55.5	162.2±0.2	−1.23			86	0.69	−11.06±0.03	−6.40 to −3.00
9.65 ±0.05	62.2	138.8±0.5	−1.63			78	0.76	−11.50±0.08	−6.40 to −3.00

ranging from 0.125M (1.2 percent) to 9.65M (62.2 percent) are summarized in Table I and in Figs. 3a and 3b. If the logarithm of the current density is plotted against the overvoltage, straight lines are obtained on all solutions (except the 5.85M) from which the constants I_0 and b (or α) in Tafel's equation can be determined. The constant b is given by the slope of the line and is equal to the rise in overvoltage accompanying a tenfold rise in current density; log I_0 is equal to the intercept on the log I axis obtained by extrapolating the line to zero overvoltage. As an illustration of the data, the Tafel plot of the experimental points for runs Nos. 1 and 3 on the 5.85M solution is given in Fig. 4 (the other runs made on this solution either coincided with the above, or fell between the two curves and are omitted from the plot). This plot is not a straight line, but has a slight concavity towards the overvoltage axis.

In Table I, the first column gives the molarity and the second the weight percentage of the H_2SO_4 solutions electrolyzed. The third column gives the potential difference: V(calomel) $- V_{Pt(H_2)}$, and the fourth the pH calculated from this potential (based on the value 471 mv for pH 4.00 as measured in 1/20M potassium hydrogen phthalate buffer), the fifth the potential difference: V(glass) $- V$(calomel) as measured in a Beckman pH meter and the sixth the corresponding pH value. The seventh, eighth, and ninth columns give the constants b, α, and log I_0 determined from the Tafel plot, and the tenth the range of log I within which these constants were observed. The values of b are obtained from the Tafel plot of the averaged values of the overvoltage, $\bar{\eta}(I)$, at intervals of 0.25 in log I. The precision measures assigned to log I_0 correspond to the spread in the overvoltage $\eta(I)$, and are based on the assumption that the value of b chosen from the slope is free of error. Actually on the 2.35M and 2.83M solutions this assumption is not justified at higher current densities (log $I > -4.25$), where the Tafel plot slopes upwards with a comparatively large scatter in the values of $\eta(I)$, and b values ranging from 115 to 150 mv are obtained on individual runs. On the 5.85M solution the Tafel plot curves upwards (see Fig. 4) and no single value of the constants can be assigned. The curve can be arbitrarily divided into short segments, each of which can be treated as a straight line. The b and log I_0 values given for this solution were obtained in this manner.

In Figs. 3a and 3b, the overvoltage $\eta(I)$ is plotted as a function of the sulfuric acid concentration expressed in terms of weight percent, for constant values of log I at intervals of 0.25 in log I in the range −6.25 to −3.00. The points represent the values of $\eta(I)$ obtained from the

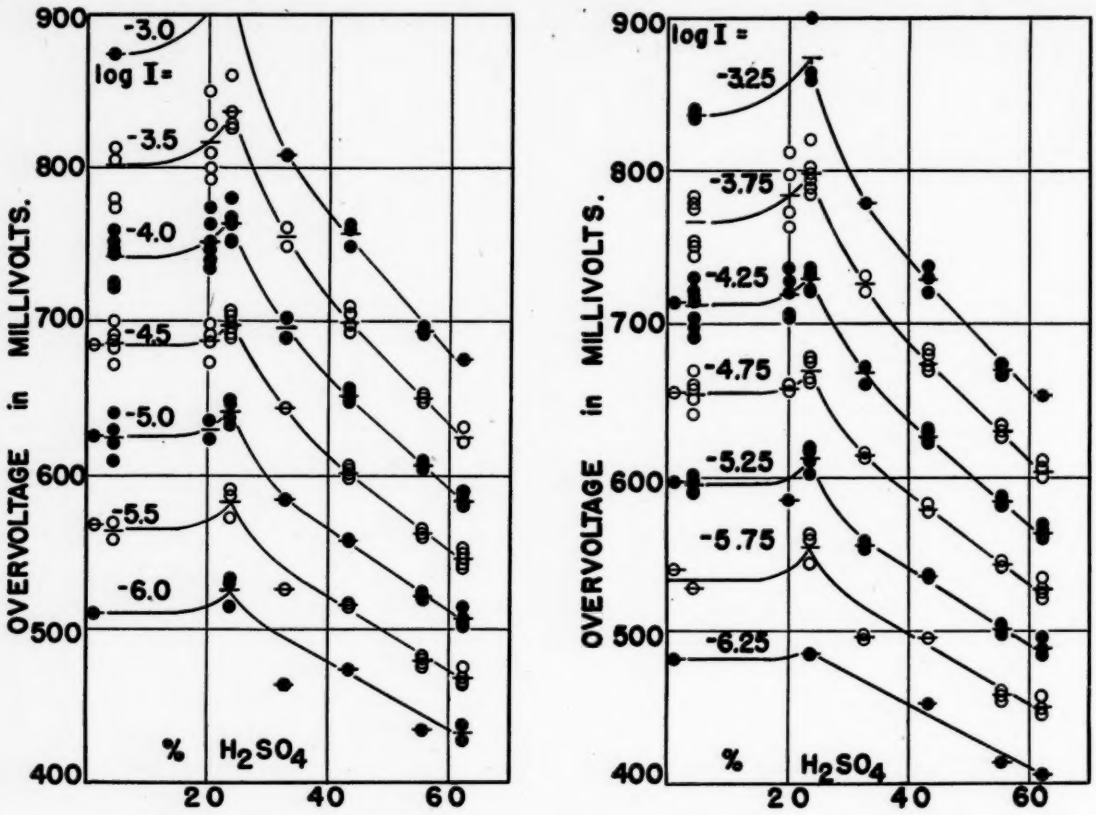

FIGS. 3a and 3b. Overvoltage at constant values of the logarithm of the current density in sulfuric acid solutions at 25°C.

several runs on each solution. The horizontal bar gives the position of the average of each cluster.

In dilute sulfuric acid solutions, the overvoltage $\eta(I)$ is independent of the acid concentration and of the *p*H, in agreement with the observations of F. P. Bowden on buffer solutions and on a dilute sulfuric acid solution in the *p*H range 0.8 to 6.6.[5] The value $\alpha=\frac{1}{2}$ is in agreement with Bowden's, while his value of $\log I_0$ on mercury (-11.2 at 25°C) is lower than that obtained here (-10.4). The overvoltage continues to obey these characteristics as the H_2SO_4 concentration is increased up to about 24 percent, at which point a slight peak (of *ca.* 15–20 mv) in the curve is noticeable. This peak becomes more pronounced at the higher current densities where α values below $\frac{1}{2}$ are obtained, and considerable unsteadiness in the $\eta(I)$ values is observed (similar to that observed by Bowden in the high current density region, and attributed by him to concentration polarization).

Beyond the "critical concentration" of *ca.* 24 percent $\eta(I)$ drops sharply. As the concentration is increased further, $\eta(I)$ continues to decrease approximately as a linear function of the weight percent, in the region 33 percent to 62 percent. This drop in the overvoltage is accompanied by

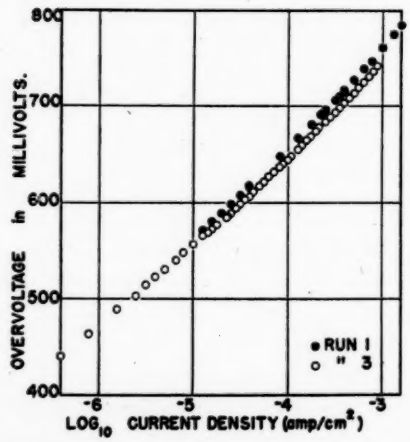

FIG. 4. Overvoltage *versus* the logarithm of the current density. Experimental points for runs Nos. 1 and 3 in 5.85*M* H_2SO_4.

TABLE II. Overvoltage measurements in phosphoric acid at 25°C.

Molarity	Weight %	Potential calomel to hydrogen mv	pH	Potential glass to calomel mv	pH	b	α	log I_0 (I_0 in amp./cm²)	Range of measurements log I
1.145±0.010	10.6	283.9±0.8	0.83		0.75	130	0.455	−10.32±0.15	−6.40 to −4.00
3.21 ±0.01	27.1	253.1±0.3	0.31		0.13	152	0.39	− 9.28±0.08	−5.50 to −3.60
5.65 ±0.03	43.3	218.5±1.3	−0.28	479.3	−0.41	226	0.26	− 7.17±0.05	−6.40 to −4.00
						191	0.31	− 7.71	−4.00 to −2.45
						266	0.22	− 6.23	−2.45 to −1.90

a progressive rise in α from $\frac{1}{2}$ to $\frac{3}{4}$, while log I_0 remains approximately constant at *ca.* $-11\pm\frac{1}{2}$.

RESULTS—PHOSPHORIC ACID SOLUTIONS

Overvoltage measurements were made in three phosphoric acid solutions with concentrations of 1.145M (10.6 percent), 3.21M (27.1 percent), and 5.63M (43.3 percent). The results are summarized in Table II and Figs. 5a and 5b. The Tafel plot gives straight lines in all cases, and the constants b and log I_0 obtained therefrom in the manner described above for sulfuric acid, are given in Table II. The data on the most concentrated of these solutions are represented schematically in Fig. 6 over the whole range of the measurements (log I from −6.40 to −1.90), the straight lines give the locus of the experimental points for the several runs on this solution. The slight break in the curve at an overvoltage of about 750 mv corresponds to the point at which the stopcock was opened between the anode and cathode compartments.

In Figs. 5a and 5b, the overvoltage $\eta(I)$ is plotted as a function of the weight percent of H_3PO_4 for constant values of log I (in the range −6.25 to −3.75). Again the overvoltage $\eta(I)$ is seen to decrease as the acid concentration is increased, but in a manner altogether different from that observed in H_2SO_4. In H_3PO_4, the curves get further apart instead of coming together, corresponding to a gradual decrease in α from a value slightly less than $\frac{1}{2}$ in the most dilute of the three solutions, to $\frac{1}{4}$ in the most concentrated, accompanied by a rise in log I_0 from −10.3 to −7.2.

DISCUSSION

The independence of the overvoltage from the pH or acid concentration, as observed by Bowden in the pH range 0.8 to 6.6, and as required by the EGL mechanism which assumes that the protons discharged come from the solvent (water), has been confirmed in dilute sulfuric acid solutions, and is found to hold up to a concentration of *ca.* 24 percent by weight (5.5 mole percent, 2.83M). There is apparently a slight peak in the overvoltage in the vicinity of this critical concentration. Beyond this point the overvoltage $\eta(I)$ drops sharply, and decreases approximately as a linear function of the weight percentage of sulfuric acid up to *ca.* 62 percent (23 mole percent), the curves of constant log I tending to come together. It is evident that in this region the EGL water mechanism breaks down, and since the water is progressively being replaced by a stronger acid, it is reasonable to expect that the discharge of protons should require less

TABLE III. Percentage ionization of sulfuric acid, from N. R. Rao's Raman data.*

Molarity	3.0	6.8	8.7	10.8	12.8	14.9	16.9
% Ionization	93.3	85.3	74.1	60.3	38.2	17.2	7.1

* There are some minor discrepancies between Rao's reported intensities and his results calculated from them, presumably owing to faulty proofreading. The numbers given in Table III are taken from the first and last columns of Rao's Table I. They agree with the points on his Fig. 2 and are, therefore, presumed to have been correctly reported.

TABLE IV. Concentration of hydrogen sulfate [H_2SO_4] and total concentration of water in the solutions used for overvoltage measurements.

Molarity	% Un-ionized	[H_2SO_4] moles/liter	Total concentration of H_2O moles/liter
0.125	0.27	0.00034	55.1
0.465	1.005	0.00468	54.5
2.35	5.08	0.119	50.6
2.83	6.105	0.172	49.4
4.16	9.00	0.374	46.4
5.85	12.65	0.74	42.0
8.2	22.5	1.85	35.2
9.65	31.5	3.04	31.9

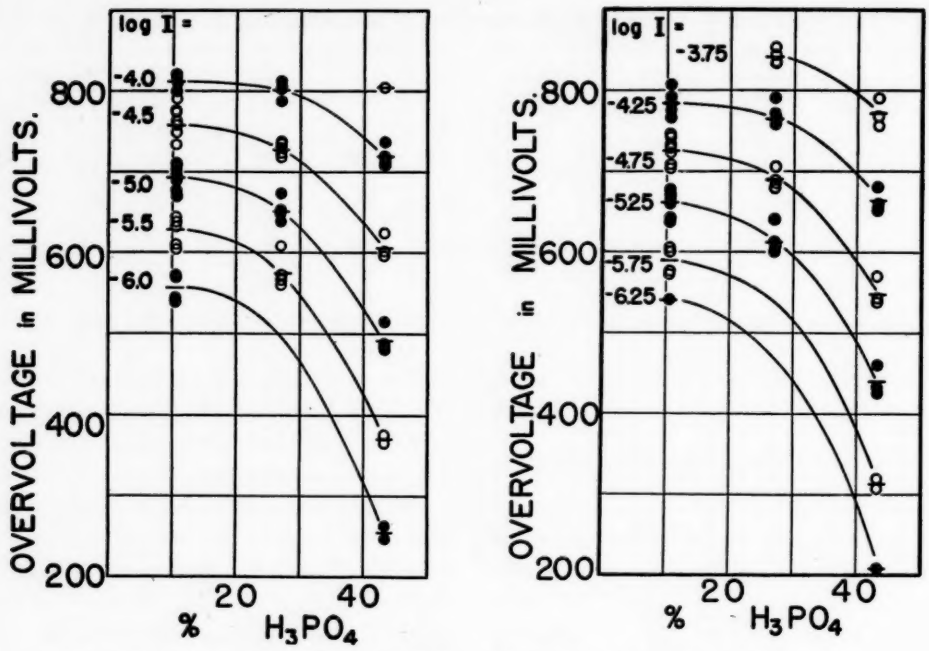

FIGS. 5a and 5b. Overvoltage at constant values of the logarithm of the current density in phosphoric acid solutions at 25°C.

activation energy, i.e., the overvoltage at a given current density $\eta(I)$ should drop. The preliminary results on phosphoric acid also show that there is a breakdown of the water mechanism as the H_3PO_4 concentration is increased, as indicated by a drop in the overvoltage. Here, however, the curves of constant log I tend to spread out further apart.

It is easy to generalize Eq. (1) to the case in which several acids compete in donating protons to the cathode, and the process is activation controlled for each. It may be assumed that the total discharge current is given by summing together the rates of proton discharge from the different acids present, i.e.,

$$I=\frac{\epsilon kT}{h}\sum_i \exp\left[\frac{\Delta S_i^{\ddagger}}{k}-\frac{\Delta H_i^{\ddagger}}{kT}-\frac{\epsilon}{kT}\sum_j \alpha_{ij}V_j\right][HB_i], \quad (11)$$

where the index i refers to the acids HB_i, and the index j refers to the several potential terms V_j entering into the total double-layer potential V, and α_{ij} is the fraction of the potential V_j that is operative in activating the discharge of a proton from the acid HB_i. Since I is given here by a sum of exponentials, its logarithm should no longer necessarily be a straight line function of the potential or of the overvoltage. However, as the potential is varied, and the different terms entering into Eq. (11) assume different values, it will generally be true that one of the terms is very much larger than the others in which case the Tafel relation still holds.

In the system H_2O-H_2SO_4, the possible acids are H_2O, H_3O^+, HSO_4^-, and H_2SO_4. In dilute solutions, H_2O is the main proton donor according to the EGL mechanism. It seems unreasonable to expect any appreciable amounts of the negative ion HSO_4^- in the adsorbed ion layer adjacent to a negative electrode, and therefore this ion is excluded from consideration as a possible source of protons. The concentration of the ions H_3O^+ in the adsorbed ion layer is equal to the charge density in that layer, and has been shown by KGG to increase with $[H^+]$, p_{H_2}, and η in such a manner as to reach a "saturated" value, which accounts for the independence of the overvoltage $\eta(I)$ on that part of the reversible potential drop which depends on the pH. Since the overvoltage does not depend on pH in solutions having a pH as high as 6, there is very strong indication that this electrically saturated

layer of H_3O^+ ions is already existent at the cathode even in the presence of such a low hydrogen ion concentration. Further increases in the hydrogen ion concentration in the body of the solution will produce only a negligible rise in the concentration of H_3O^+ in the adsorbed ion layer. If in these solutions of relatively high pH, the oxonium ions contribute only a negligible fraction of the discharge current I, they will not contribute any more to the discharge current when the pH of the solution is lowered. There remains the acid H_2SO_4. The break in the overvoltage when the acid concentration is increased must, therefore, be attributed to the contribution of the acid H_2SO_4 to the discharge current. The values of α ($\frac{1}{2}$ to $\frac{3}{4}$) and log I_0 ($-11\pm\frac{1}{2}$) obtained in the high concentration region are then characteristic for the discharge reaction involving H_2SO_4 in the presence of water as a diluent.

This hypothesis can be tested by means of the Raman data on H_2SO_4-H_2O solutions. Of the five principal bands occurring in the sulfuric acid spectrum, it has been possible to attribute three to definite molecular species ($\Delta\nu$ 910 cm^{-1} to H_2SO_4, 980 to $SO_4^=$, and 1043 to HSO_4^-).[8] N. Rajeswara Rao's[9] measurements of the intensity of these three bands in solutions of different molarities make it possible to determine the actual concentration of the three species H_2SO_4, HSO_4^-, and $SO_4^=$ in a solution of any given molarity. His values of the "percentage ionization" (i.e., the sum of the concentrations of HSO_4^- and $SO_4^=$ as a fraction of the molarity) are reproduced in Table III. Unfortunately, Rao does not give the temperature of his solutions, beyond stating that the cell was cooled in a stream of running water during the long exposures (5 hours). A smooth curve was drawn through the points of Table III and extended to 100 percent ionization at zero molarity. From this curve, the percentage ionization was read off for each one of the solutions used in the present research, and the actual concentration of unionized sulfuric acid (hydrogen sulfate) calculated (Table IV). The last column gives the stoichiometric concentration of water as calculated from the weight percent and the density of the solution, and includes the water taken up in the formation of oxonium ions H_3O^+.

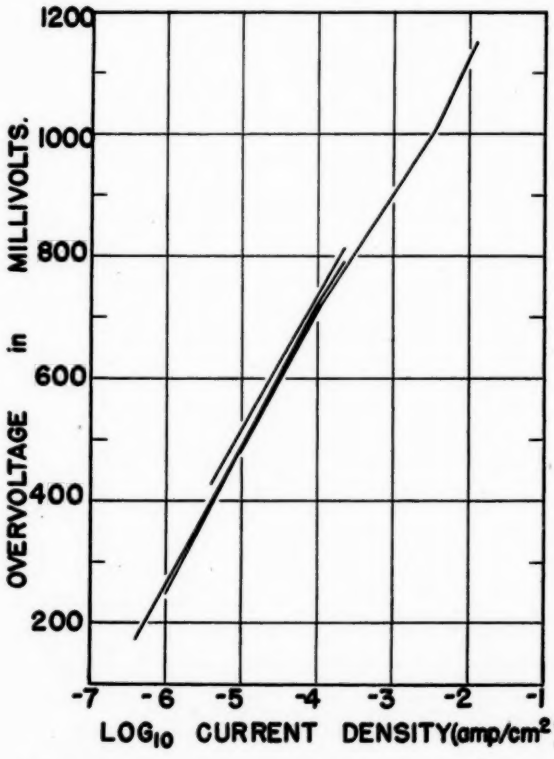

FIG. 6. Overvoltage *versus* the logarithm of the current density in 5.65M H_3PO_4. The straight line segments give the locus of the experimental points.

If the total current density is given by the sum of two terms, one caused by the discharge of protons from H_2O, the other caused by the discharge of protons from H_2SO_4, as postulated by Eq. (11), then at constant overvoltage, the dependence of I on the composition should be expressible by an equation of the form:

$$I=k_1[H_2O]+k_2[H_2SO_4], \qquad (12)$$

where the k's are constant at a given overvoltage. If the water term is small compared to the hydrogen sulfate term, this is tantamount to saying that the current density is proportional to the concentration of hydrogen sulfate in the solution. That this is actually the case is shown by Figs. 7 to 10, which give a plot of the current density I as a function of $[H_2SO_4]$ (from Table IV) for overvoltages of 509, 568, 627, and 686 mv, respectively. I is proportional to hydrogen sulfate concentration except in the dilute solutions

[8] J. H. Hibben, *The Raman Effect and Its Chemical Applications* (Reinhold Publishing Corporation, New York, 1939), p. 356 ff.

[9] N. Rajeswara Rao, Ind. J. Phys. **14**, 143 (1940).

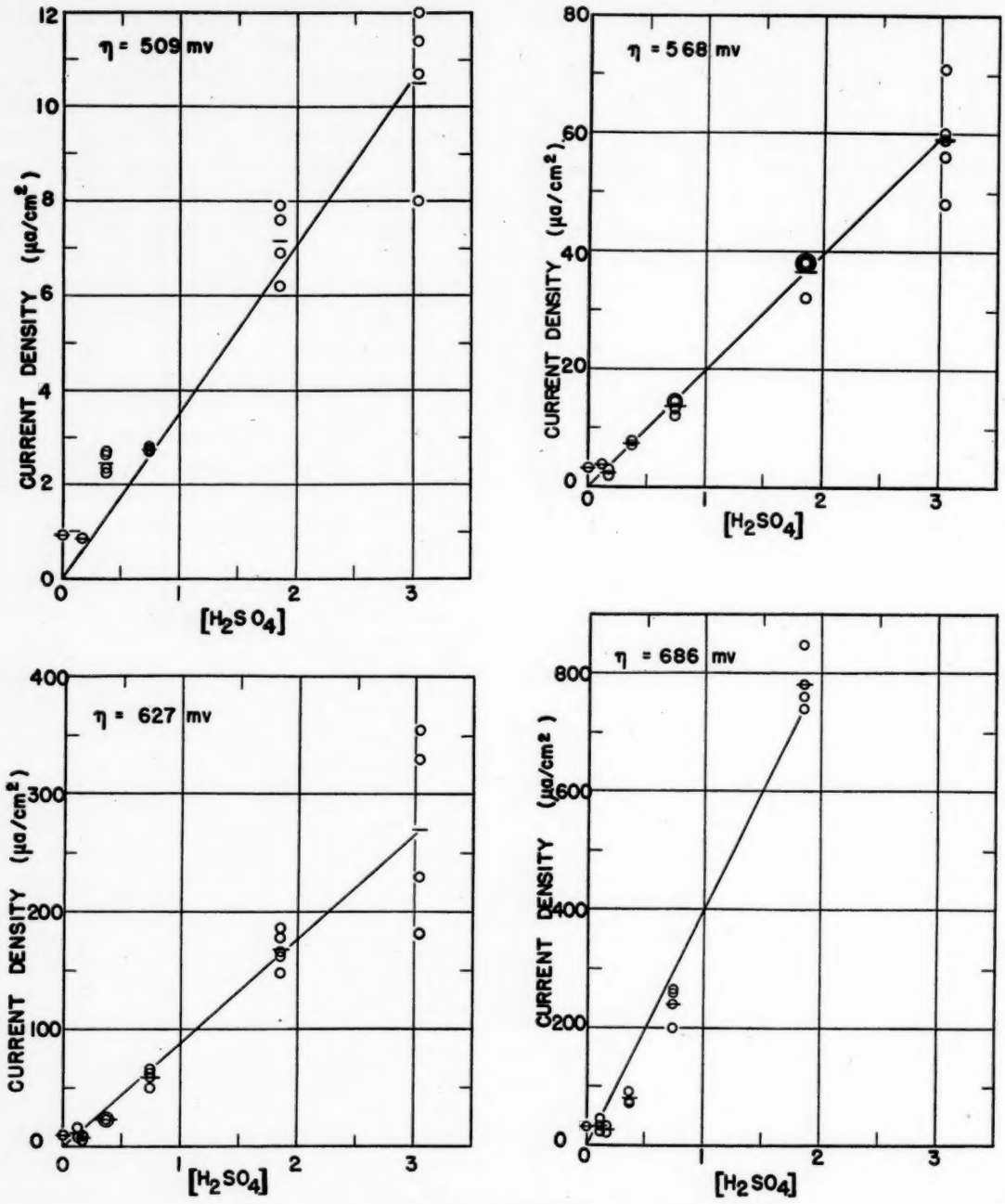

FIGS. 7–10. Current density *versus* concentration of hydrogen sulfate at overvoltages of 509, 568, 627, and 686 millivolts.

where the water current becomes an appreciable fraction of the whole, and I curves upwards away from the straight line. In the 4.16M solution the currents from the two sources are roughly equal.

It is therefore fairly conclusively proven that the discharge reaction in the more concentrated solutions involves the hydrogen sulfate molecule. This reaction has been interpreted in the above argument as the discharge of a proton from H_2SO_4. The possibility that the reaction may actually be the reduction of H_2SO_4 to H_2SO_3 has not been eliminated either theoretically or experimentally, and may account for the markedly

different α and log I_0 values in the concentrated H_2SO_4 and H_3PO_4 solutions.

In the system H_2O-H_3PO_4, the possible acids are H_2O, H_3O^+, $H_2PO_4^-$, $HPO_4^=$, and H_3PO_4. The ions can be excluded from consideration for the reasons previously given for sulfuric acid. The lowering of the overvoltage in the concentrated solutions can therefore be attributed to the discharge of protons from the acid H_3PO_4. This process is characterized by values of α less than $\frac{1}{2}$ ($\frac{1}{2}$ to $\frac{1}{4}$) and log I_0 larger than those for water (-10 to -7). This is entirely reasonable since the energy of activation should be lower for H_3PO_4 than for H_2O corresponding to the higher value of log I_0. At the same time, if the potential energy curve for a proton in the H_3PO_4 molecule lies higher than that for a proton in H_2O, the activated state should move outward, away from the electrode corresponding to the lower value of α.

THE JOURNAL OF CHEMICAL PHYSICS VOLUME 13, NUMBER 2 FEBRUARY, 1945

Amphipathic Character of Proteins and Certain Lyophile Colloids as Indicated by Absorption Spectra of Dyes*

S. E. SHEPPARD AND A. L. GEDDES
Research Laboratories, Eastman Kodak Company, Rochester, New York

(Received November 18, 1944)

A characteristic change of spectral absorption of certain dyes as between water and organic solvents is shown to appear in aqueous solutions of *gelatin* or of the colloidal detergent, *cetyl pyridinium chloride*. This behavior is attributed to a bilateral character of lamellar micelles of such bodies, the elementary lamellae being polar and hydrophile on one side, non-polar and organophile on the reverse side. The possibility is indicated of diagnosing such amphipathic characteristics by comparative spectrophotometric measurements with suitable dyes.

MANY dyes, both acid and basic, and of all types and classes[1] give in aqueous solution an absorption spectrum differing considerably from that in organic solvents. The absorption in water does not follow Beer's law, and the distribution of intensity of absorption depends upon the concentration and the temperature. A characteristic and outstanding example is given by the cyanine dye, Pinacyanol, of which the alcoholic and the aqueous absorption spectra are shown in Fig. 1.

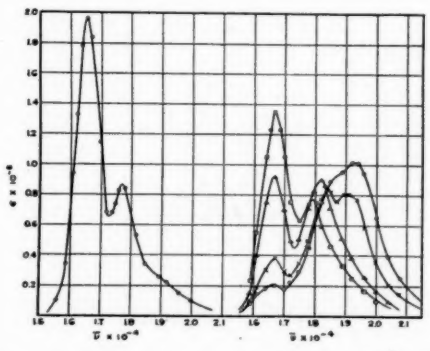

FIG. 1. Spectral absorption of Pinacyanol. Left side, in methyl alcohol. Right side, in water; ○—$4.65\times10^{-4}M$, x—$1.0\times10^{-4}M$, △—$1.0\times10^{-5}M$, □—$1.0\times10^{-6}M$.

In the course of an investigation on the diffu-

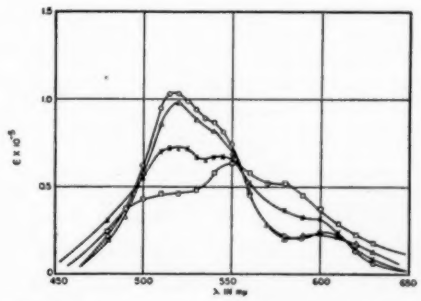

FIG. 2. Spectral absorption of Pinacyanol. Concentration $=2.7\times10^{-4}M$, temperature $=25°C$. ○—in aqueous solution—1 hr., x—in 0.6 percent aqueous gelatin solution—1 hr., △—in aqueous solution—1 week, □—in 0.6 percent aqueous gelatin solution—1 week.

* Communication No. 1000 from the Kodak Research Laboratories.

[1] S. E. Sheppard, Rev. Mod. Phys. **14**, 303 (1942); S. E. Sheppard and A. L. Geddes, J. Am. Chem. Soc. **66**, 1995–2002 (1944.)

TABLE I. Effect of gelatin on extinctions of band maxima of Pinacyanol chloride solutions—1 hour old. Temperature, 25°C.

Dye concentration (M)	$\epsilon \times 10^{-5}$ Aqueous solution α	β	γ	0.6 percent aqueous gelatin solution α	β	γ
9.0×10^{-4}	0.15	0.72	1.07	0.30	0.66	0.95
2.7×10^{-4}	0.22	0.87	1.04	0.32	0.67	0.73
1.0×10^{-4}	0.40	0.92	0.87	0.40	0.72	0.62
1.0×10^{-5}	0.98	0.95	—	0.88	0.76	—

TABLE II. Effect of gelatin on extinctions of band maxima of Pinacyanol chloride solutions—1 week old. Temperature, 25°C.

Dye concentration (M)	$\epsilon \times 10^{-5}$ Aqueous solution α	β	γ	0.6 percent aqueous gelatin solution α	β	γ
0.9×10^{-4}	0.16	0.69	1.07	0.50	0.59	0.65
2.4×10^{-4}	0.23	0.75	0.97	0.51	0.63	0.47
0.9×10^{-5}	0.37	0.82	0.80	0.58	0.64	0.40

TABLE III. Effect of C.P.C. on extinctions of band maxima of Pinacyanol chloride solutions—1 hour old. Temperature, 25°C.

Dye concentration (M)	$\epsilon \times 10^{-5}$ Aqueous solution α	β	γ	0.6 percent aqueous C.P.C. solution α	β	γ
1.0×10^{-6}	1.38	0.77	—	1.38	0.68	—
1.0×10^{-5}	0.95	0.95	—	1.06	0.66	—
1.0×10^{-4}	0.40	0.93	0.88	0.59	0.69	0.52
2.7×10^{-4}	0.26	0.87	1.04	0.38	0.63	0.55
9.0×10^{-4}	0.15	0.73	1.07	0.27	0.56	0.65
1.8×10^{-3}	—	—	1.10	—	0.54	0.75

sion of dyes and electrolytes, we had occasion to determine the absorption spectrum of Pinacyanol in aqueous gelatin solutions. In the presence of gelatin, the absorption spectrum deviates from that in pure water, at the same concentration of dye. Furthermore, the deviation is such that the spectrum approaches that in organic solvents (cf. Fig. 1). This behavior is illustrated in Tables I and II, and in Fig. 2 (at one concentration only).

It is apparent that the presence of gelatin favors the "organic" spectrum $\epsilon_\alpha > \epsilon_\beta > \epsilon_\gamma$, and that there is an "aging" factor associated with this change in the presence of gelatin. (The change with time in the simple aqueous solution merely indicates a slight total fading of the dye.) Such a redistribution of the spectrum would be expected if the gelatin were so (incompletely) dispersed that its particles afforded, in part at any rate, a non-polar organic aspect in which adsorbed dye could dissociate as in a layer of organic solvent. The possibility of an electrochemical combination of the dye and the (charged) gelatin[2] was avoided by using an acid-process gelatin of high isoelectric point (pH = *ca.* 8.8). Consequently, at the pH of operation (pH = *ca.* 5.6), both the dye (cation) and the gelatin would be positively charged, and there would be no electrochemical (electrostatic) attraction between them. Reasoning in this way, it appeared to us that a similar behavior to that of gelatin should be shown by such micelle-forming bodies as macromolecular detergents and spreading agents. Data obtained with the same dye (Pinacyanol) in aqueous solutions of *cetyl pyridinium chloride* (C.P.C.) appear to confirm the idea. See Table III and Fig. 3.

It is evident that the cetyl pyridinium compound behaves in a manner similar to that of gelatin, and, for the same percentage concentration,[3] rather more strongly. In both cases the addition of a micelle-forming hydrophile colloid effects conversion of some of the dye from an aggregated—probably dimeric—to a monomeric state.

This points to the partition of the dye between two phases, water, and micelles of the colloid. At first sight it might seem that a sufficient picture of the process involved would be to assume a polar non-polar "amphipathic" dye

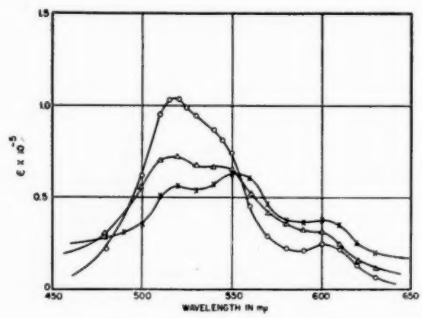

FIG. 3. Spectral absorption of Pinacyanol. Concentration $= 2.7\times10^{-4}M$, temperature = 25°C. ○—in aqueous solution—1 hr., x—in aqueous solution 0.6 percent C.P.C. solution—1 hr., △—in aqueous solution 0.6 percent gelatin solution—1 hr.

[2] S. E. Sheppard, R. C. Houck, and C. Dittmar, J. Phys. Chem. **46**, 158 (1942).

[3] As yet, they cannot be compared on a molar basis.

molecule or ion, symbolically expressed by ⊣O, and that the non-polar, organophile end penetrates an oil-like globule or micelle of the colloid, so that "dimerization" of the dye ions is prevented. However, on consideration of the structure of most dye molecules, it appears that this image is geometrically inadequate. The dye molecules are not linear, but *planar* structures; one edge of the planar unit may be regarded as containing one (or more) ionic (or polar) centers, and is thereby hydrophile, while the remainder is essentially non-polar and organophile.[4] Of this amphipathic configuration, it is the dorsal, organophile edge or plane which would have to be attracted to, and cohere with, a corresponding portion of the colloid.

This appears to us to be consistent with a *lamellar* rather than a *spheroidal* configuration for a colloid micelle, whether of gelatin or of the detergent.[5] As supporting this conclusion, it may be pointed out that both the dye and the colloid or detergent are cations. If the colloid particles were spheroidal, the outer surface would be expected to be hydrophile and positively charged. This would produce a strong potential barrier hindering the dye from penetrating the colloid,[2] whereas with a lamellar two-faced configuration, the common organophile portions can readily cohere.

As more spectroscopic data for varying types of dye molecules (of differing constitutions, sizes, and shapes) become available, a new tool for the investigation of the micellar organization of colloids will be at hand.

There are certain interesting contacts and relations between the phenomena just described and those of the "solubilization" of dyes recently discussed by McBain[6] and his collaborators, and also with the adsorption of dyes and proteins to silver halides.[7] It is hoped to present further evidence shortly on these aspects of the subject.

[4] S. E. Sheppard, Atti del X Congr. Intern. di Chimica (Rome) **1**, 234 (1938).
[5] D. G. Dervichian, J. Chem. Phys. **11**, 236 (1943).
[6] J. W. McBain and K. E. Johnson, J. Am. Chem. Soc. **66**, 9 (1944).
[7] S. E. Sheppard, R. H. Lambert, and R. D. Walker, J. Chem. Phys. **7**, 265 (1939).

THE JOURNAL OF CHEMICAL PHYSICS VOLUME 13, NUMBER 2 FEBRUARY, 1945

A Generalization of the Quasi-Chemical Method in the Statistical Theory of Superlattices

C. N. YANG*
National Tsing Hua University, Kunming, China
(Received November 17, 1944)

The quasi-chemical method in the investigation of the equilibrium distribution of atoms in the pairs of neighboring sites in a superlattice is generalized by considering groups containing large numbers of sites. The generalized method may be used to obtain successive approximations of the free energy of the crystal. The labor of integration is avoided by the introduction of a Legendre transformation. In order to analyze the fundamental assumption underlying the method more closely, the number of arrangements of the atoms for given long-distance order is calculated and the hypothesis of the non-interference of local configurations discussed. The method is applied to the calculation of the free energy in the different approximations discussed in this paper, including Bethe's second approximation and a simple approximation for the face-centered cubic crystal Cu_3Au.

1. INTRODUCTION

IT was shown by Fowler and Guggenheim[1] that the quasi-chemical method, originally devised for the theory of regular solutions, applies equally well to the theory of superlattices with long-distance order. The method is, as they have emphasized, definitely one stage further towards an exact theory than Bragg-Williams' method.[2] Compared with Bethe's[3] or Kirkwood's[4] method it also distinguishes itself in mathematical simplicity. But in its original form the method does not lead to a consistent scheme of successive approximations and cannot be regarded as a method of approach towards the rigorous evaluation of the configurational free energy of an alloy. In the present paper a new formulation of the quasi-chemical method is developed which is capable of yielding successively higher approximations.

The free energy expression in both Bethe's method and the quasi-chemical method involves an integral. Its evaluation is very complicated and has been carried out[1,5] so far only in Bethe's approximation for simple and body-centered cubic crystals. In the new formulation of the quasi-chemical method, however, it will be shown that a Legendre transformation helps to effect the integration. (It might be noticed that a similar Legendre transformation is used to essentially the same effect in Fowler's formulation of general statistical mechanics. Compare Fowler.[6]) The free energy is obtained directly as a closed expression. Its values are given for Bethe's first and second (modified) approximations and for the face-centered alloy Cu_3Au in Sections 7 and 8.

To make sure that the quasi-chemical method may actually be used to obtain a series of successively better approximations, we must investigate the free energy in high order approximations and compare it with the partition function of the crystal. This is done in Section 5 together with a comparison of the quasi-chemical and Bethe's methods.

Except in the last section we shall be concerned only with binary alloys with atomic ratio 1:1 forming a (quadratic), simple cubic, or body-centered cubic lattice. The generalization of the method to the investigation of alloys with other atomic ratios and forming other types of lattices is easy. In fact, the superior power of the quasi-chemical method appears to be even more fully revealed when a face-centered lattice is studied. This problem is taken up at the end of the paper where an approximate free energy

* Research Fellow of the China Foundation for the Promotion of Education and Culture.

[1] R. H. Fowler and E. A. Guggenheim, Proc. Roy. Soc. **A174**, 189 (1940).

[2] W. L. Bragg and E. J. Williams, Proc. Roy. Soc. **A145**, 699 (1934); **151**, 540 (1935); **152**, 231 (1935).

[3] H. A. Bethe, Proc. Roy. Soc. **A150**, 552 (1935).

[4] J. G. Kirkwood, J. Chem. Phys. **6**, 70 (1938).

[5] T. S. Chang, Proc. Camb. Phil. Soc. **35**, 265 (1939); J. G. Kirkwood, J. Chem. Phys. **8**, 623 (1940); J. S. Wang, "Free energy in the statistical theory of order-disorder transformation," Science Report of National Tsing Hua University, Series A, 30th Anniversary Memorial Number (1941), printed but failed to appear.

[6] R. H. Fowler, *Statistical Mechanics*, second edition, p. 188.

expression for Cu_3Au is obtained and its critical phenomena discussed.

2. REFORMULATION OF THE QUASI-CHEMICAL METHOD

Consider an alloy of type AB with altogether $N=2N_1$ atoms. Let z be the number of nearest neighbors of each atom. Those sites in the superlattice occupied by the A atoms at the absolute zero of temperature will be called the α-sites, and the rest, the β-sites. The partition function of the crystal may be written in the form

$$\sum_w P(w, T), \tag{1}$$

where $P(w, T)$ is equal to $e^{-E/kT}$ summed over all possible configurations of the crystal having N_1w α-sites occupied by B (wrong) atoms. The average energy over all these configurations is

$$\bar{E}(w, T)=kT^2\frac{\partial}{\partial T}\log P(w, T). \tag{2}$$

But evidently

$$P(w, \infty)=g(w)=\left[\frac{N_1!}{(N_1w)!(N_1-N_1w)!}\right]^2. \tag{3}$$

Hence

$$\log P(w, T)=\log g(w)+\int_\infty^T \frac{1}{kT^2}\bar{E}(w, T)dT. \tag{4}$$

The problem of finding the partition function of the crystal therefore reduces to one of finding $\bar{E}(w, T)$. An approximate solution has been obtained by Fowler and Guggenheim. Their method will now be presented in a new form better suited to generalization.

There are in the crystal zN_1 pairs of nearest neighboring sites $\alpha-\beta$. Let $[q_\alpha, q_\beta]$ of these be occupied by $q_\alpha(=0, 1)$ wrong (B) atoms on the α-site and $q_\beta(=0, 1)$ wrong (A) atoms on the β-site. For given w the following relations hold:

$$\begin{aligned}[0, 0]+[0, 1]+[1, 0]+[1, 1]&=zN_1,\\ [1, 0]+[1, 1]&=zN_1w,\\ [0, 1]\qquad\quad+[1, 1]&=zN_1w.\end{aligned} \tag{5}$$

Upon the approximation of the nearest neighbor interaction the energy of the crystal may be written as

$$\begin{aligned}E(r, T)=&[0, 0]V_{AB}+[0, 1]V_{AA}\\ &+[1, 0]V_{BB}+[1, 1]V_{AB},\end{aligned} \tag{6}$$

where the V's are the interaction energies between the different kinds of pairs of nearest neighbors.

We may give (5) and (6) a different interpretation by imagining $[0, 0]$, $[0, 1]$, $[1, 0]$, $[1, 1]$ and V_{AB}, V_{AA}, V_{BB}, V_{AB} to be, respectively, the numbers and the molecular internal energies of four different kinds of molecules, say, X, XZ, XY, XYZ of a gaseous assembly. The interpretation of (6) is that the assembly has the same internal (non-kinetic) energy as the crystal at the given value of w. Equation (5) would mean that the total numbers of X, Y, Z atoms are, respectively, zN_1, zN_1w, zN_1w.

The quasi-chemical method consists in taking the averages $\langle 0, 0\rangle_{Av}$, $\langle 0, 1\rangle_{Av}$, $\langle 1, 0\rangle_{Av}$, $\langle 1, 1\rangle_{Av}$ of the chemical assembly at any temperature as approximately representing the corresponding averages of the crystal at the same temperature.

A detailed treatment of the problem of a gaseous assembly has been given by Fowler.[7] We are only interested in our assembly of four different kinds of molecules, for which the results may be summarized as:

$$\begin{aligned}\langle 0, 0\rangle_{Av}&=\xi \exp\left[-V_{AB}/kT\right],\\ \langle 0, 1\rangle_{Av}&=\xi\nu \exp\left[-V_{AA}/kT\right],\\ \langle 1, 0\rangle_{Av}&=\xi\mu \exp\left[-V_{BB}/kT\right],\\ \langle 1, 1\rangle_{Av}&=\xi\mu\nu \exp\left[-V_{AB}/kT\right],\end{aligned} \tag{7}$$

where ξ, μ, and ν are to be determined from (6).

In Fowler and Guggenheim's work the starting point is the equation

$$\begin{aligned}\langle 0, 0\rangle_{Av}\langle 1, 1\rangle_{Av}/\langle 0, 1\rangle_{Av}\langle 1, 0\rangle_{Av}&\\ =\exp\left[(V_{AA}+V_{BB}-2V_{AB})/kT\right],&\end{aligned} \tag{8}$$

which can be obtained by eliminating ξ, μ, and ν from our equation (7). We shall, however, make use of (7) instead of (8) to obtain the free energy by means of a Legendre transformation which enables us to avoid the labor of integration. It will appear that this procedure is applicable to the general case studied in this paper.

In order to calculate the free energy from (4) we first write the energy of the crystal in the

[7] R. H. Fowler, *Statistical Mechanics*, second edition, pp. 162–163.

form

$$\bar{E}(w, T)=kT^2\frac{\partial}{\partial T}\phi(\xi, \mu, \nu, T),$$

where

$$\phi(\xi, \mu, \nu, T)=\xi \exp[-V_{AB}/kT]+\xi\nu \exp[-V_{AA}/kT]+\xi\mu \exp[-V_{BB}/kT]+\xi\mu\nu \exp[-V_{AB}/kT].$$

From (5) it is evident that

$$\xi\frac{\partial\phi}{\partial\xi}=zN_1, \quad \mu\frac{\partial\phi}{\partial\mu}=zN_1w, \quad \nu\frac{\partial\phi}{\partial\nu}=zN_1w.$$

If these last three equations are regarded as defining ξ, μ, and ν in terms of w and T, i.e., if the Legendre transformation:

$$\log\xi, \log\mu, \log\nu, T\rightarrow zN_1, zN_1w, zN_1w, T$$

is made, the derivative of the function

$$\Psi(w, T)=\phi-zN_1\log\xi-zN_1w\log\mu-zN_1w\log\nu,$$

with respect to T is found to be

$$\frac{\partial\Psi}{\partial T}=\frac{\partial\phi}{\partial T}=\frac{1}{kT^2}\bar{E}(w, T).$$

This shows that the integral in (4) may be expressed directly as a function of ξ, μ, ν and T:

$$\int_\infty^T\frac{1}{kT^2}\bar{E}(w, T)dT=\Psi(w, T)-\Psi(w, \infty).$$

The values of the parameters at $T=\infty$ are easily determined from (5) and (7):

$$\xi=zN_1(1-w)^2, \quad \mu=\nu=\frac{w}{1-w}.$$

Thus (4) becomes

$$\log P(w, T)=2\log\frac{N_1!}{(N_1w)!\{N_1(1-w)\}!}+zN_1\log\frac{zN_1(1-w)^2}{\xi}+zN_1w\log\frac{w^2}{(1-w)^2\mu\nu},$$

so that the free energy of the crystal is

$$F_0(w, T)=-kT\log P(w, T)=-kT\{zN_1\log zN_1+2(z-1)N_1[w\log w+(1-w)\log(1-w)]-zN_1\log\xi-zN_1w\log\mu\nu\}. \quad (9)$$

We shall have occasion to return to this expression for the free energy later in Section 4.

3. GENERALIZATION TO GROUPS OF FOUR SITES

So far our attention has been fixed on the pairs of nearest neighbors in the crystal. They are classified into four different kinds and the average number of pairs in each class is obtained from chemical analogy. Now we shall generalize the whole procedure by taking into consideration all the groups of sites of a certain arbitrarily chosen form in the crystal. These groups will be classified according to the way they are occupied by atoms and the average number of groups in each class is to be obtained by chemical analogy.

To make this clear let us consider in detail groups of four sites forming the corners of squares (as shown in Fig. 1) in a quadratic lattice. We

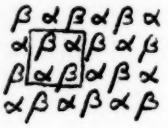

FIG. 1.

classify these groups into $2^4=16$ classes and denote them by (0, 0, 0, 0), (0, 0, 0, 1), $\cdots$, (1, 1, 1, 1), respectively, so that all groups in the class (q_1, q_2, q_3, q_4) have q_1 wrong atoms in their upper α-sites, q_2 wrong atoms in their lower α-sites, q_3 wrong atoms in their upper β-sites, and q_4 wrong atoms in their lower β-sites. The total number of these groups is N, hence if we denote the number of groups in the class (q_1, q_2, q_3, q_4) by $[q_1, q_2, q_3, q_4]$,

$$\sum_{q_i=0}^{1}[q_1, q_2, q_3, q_4]=N_1. \quad (10)$$

Now the number of all those groups in the crystal with a wrong atom on the upper α-site is just the number of wrong atoms on the α-sites. Similar reasoning may be applied to the other three sites, so we obtain

$$\sum_q q_i[q_1, q_2, q_3, q_4]=N_1w, \quad i=1, 2, 3, 4. \quad (11)$$

Let $\chi(q_1, q_2, q_3, q_4)$ be the energy of each group in the class (q_1, q_2, q_3, q_4). It is easy to show that

$$\chi=(2-q_1-q_2)(q_3+q_4)V_{AA}+\{(2-q_1-q_2)(2-q_3-q_4)+(q_1+q_2)(q_3+q_4)\}V_{AB}+(2-q_3-q_4)(q_1+q_2)V_{BB}.$$

The total energy of the crystal is given in terms of $\chi(q_1, q_2, q_3, q_4)$ by

$$E(w, T)=\sum_q [q_1, q_2, q_3, q_4]\chi(q_1, q_2, q_3, q_4). \quad (12)$$

We may give (10), (11), and (12) interpretations similar to those given in Section 2 for Eqs. (5) and (6). The same quasi-chemical method used there to obtain (7) leads now to the following averages for given w:

$$\langle q_1, q_2, q_3, q_4\rangle_{Av}=\xi\mu_1^{q_1}\mu_2^{q_2}\mu_3^{q_3}\mu^{q_4} \times\exp[-\chi(q_1, q_2, q_3, q_4)/kT]. \quad (13)$$

In this expression the parameters ξ, μ_1, μ_2, μ_3, and μ_4 are to be determined from (10) and (11), which may be written in the form

$$\xi\frac{\partial\phi}{\partial\xi}=N_1, \quad \mu_i\frac{\partial\phi}{\partial\mu_i}=N_1w, \quad (i=1, 2, 3, 4) \quad (14)$$

if we put

$$\phi(\xi, \mu_1, \mu_2, \mu_3, \mu_4)=\sum_q \xi\mu_1^{q_1}\mu_2^{q_2}\mu_3^{q_3}\mu_4^{q_4} \times\exp[-\chi(q_1, q_2, q_3, q_4)/kT]. \quad (15)$$

It can be shown[8] that ξ and μ_i are uniquely determined by (14) at given w and T. Their values at $T=\infty$ are

$$(\xi)_{T=\infty}=N_1(1-w)^4,$$

$$(\mu_i)_{T=\infty}=\frac{w}{1-w}, \quad i=1, 2, 3, 4; \quad (16)$$

as can be shown by substitution into (14).

To calculate the free energy it is necessary first to evaluate the integral in (4). By (12) and (13) the integrand may be written as

$$\frac{1}{kT^2}\bar{E}(w, T)=\frac{1}{kT^2}\sum_q \langle q_1, q_2, q_3, q_4\rangle_{Av} \times\chi(q_1, q_2, q_3, q_4)=\frac{\partial\phi}{\partial T}, \quad (17)$$

where the partial differentiation is to be taken with ξ, μ_1, μ_2, μ_3, μ_4, and T as the independent variables. If, however, we regard them as functions of w and T defined by (14) and introduce the Legendre transformation

$$\log\xi, \log\mu_1, \log\mu_2, \log\mu_3, \log\mu_4 \rightarrow N_1, N_1w, N_1w, N_1w, N_1w, \quad (18)$$

(17) reduces to

$$\frac{1}{kT^2}\bar{E}(w, T)=\frac{\partial\phi}{\partial T}=\frac{\partial}{\partial T}\Psi(w, T), \quad (19)$$

where the function Ψ is defined by

$$\Psi=\phi-N_1\log\xi-\sum_i N_1w\log\mu_i. \quad (20)$$

Substituting (19) into (4) we get

$$\log P(w, T)=\log g(w)+\Psi(w, T)-\Psi(w, \infty), \quad (21)$$

so that the free energy may be written down directly as

$$F(w, T)=-kT\log P(w, T) =-kT[\log g(w)+\Psi(w, T)-\Psi(w, \infty)]. \quad (22)$$

The equilibrium value $\bar{w}$ of w is obtained by minimizing F, so we have

$$0=\frac{\partial}{\partial\bar{w}}F(\bar{w}, T)=-kT\left[\frac{d}{d\bar{w}}\log g(\bar{w}) +\frac{\partial}{\partial\bar{w}}\Psi(\bar{w}, T)-\frac{\partial}{\partial\bar{w}}\Psi(\bar{w}, \infty)\right]. \quad (23)$$

But by (14) and (20)

$$\frac{\partial}{\partial w}\Psi(w, T)=-\sum_i N_1\log\mu_i,$$

and by (3)

$$\frac{d}{dw}\log g(w)=-2N_1\log\frac{w}{1-w},$$

so by (16)

$$\sum_i \log\mu_i=-2\log\frac{\bar{w}}{1-\bar{w}} +[\sum_i \log\mu_i]_{T=\infty}=2\log\frac{\bar{w}}{1-\bar{w}};$$

i.e.,

$$\prod_i \mu_i=\left(\frac{\bar{w}}{1-\bar{w}}\right)^2. \quad (24)$$

[8] The proof follows easily from Lemma 2.42 in Fowler's *Statistical Mechanics*, second edition.

It will be shown in the next section that we may put $V_{AA}=V_{BB}$, and $V_{AB}=0$ without altering the specific heat of the crystal if

$$V=\tfrac{1}{2}(V_{AA}+V_{BB})-V_{AB}$$

is left unchanged. When this is done, ϕ will be symmetrical with respect to μ_1, μ_2, μ_3, and μ_4, and we conclude that all the μ's are equal, because: (i) Eq. (14) has only one set of solutions; and (ii) if the conclusion is true, (14) becomes, with all μ_i put equal to μ,

$$\xi\frac{\partial\phi}{\partial\xi}=N_1, \quad \mu\frac{\partial\phi}{\partial\mu}=4N_1w, \tag{25}$$

which *does* have a set of solutions in ξ and μ. Now ϕ is given by

$$\phi=\xi[1+4\mu x^2+(4\mu^2x^2+2\mu^2x^4)+4\mu^3x^2+\mu^4], \tag{26}$$

where

$$x=\exp\left[-\tfrac{1}{2}(V_{AA}+V_{BB}-2V_{AB})/kT\right]. \tag{27}$$

Introducing the degree of order s by $s=1-2w$ and eliminating ξ from (25), we obtain

$$(1+s)\mu^4+(2+4s)\mu^3x^2+2sx^2(x^2+2)\mu^2 +(4s-2)x^2\mu+(s-1)=0. \tag{28}$$

The free energy is given by (16) and (22):

$$\frac{-F(w,T)}{2N_1kT}=(1-w)\log(1-w) +w\log w-2w\log\mu+\tfrac{1}{2}\log(1+4\mu x^2 +4\mu^2x^2+2\mu^2x^4+4\mu^3x^2+\mu^4), \tag{29}$$

and the condition of equilibrium by (24):

$$\mu=\left(\frac{1-s}{1+s}\right)^{\frac{1}{2}}. \tag{30}$$

To obtain the critical temperature, we expand (28) in powers of s and find, after identifying coefficients,

$$\log\mu=-\frac{1+6x^2+x^4}{2+2x^2}s+Ks^3+\cdots$$

which is the only real solution for $\log\mu$. Next we expand (30);

$$\log\mu=-s-\tfrac{1}{3}s^3-\cdots.$$

At the critical value x_c of x, these last two equations have a multiple solution at $s=0$. Hence

$$-\frac{1+6x_c^2+x_c^4}{2+2x_c^2}=-1,$$

i.e.,

$$x_c=(\sqrt{5}-2)^{\frac{1}{2}}=0.4858.$$

4. GENERAL FORM OF THE QUASI-CHEMICAL METHOD

Let us now take a group of any size and form. Let it have a α-sites, b β-sites, and γ pairs of nearest neighbors. The procedures to obtain an approximate expression for the free energy of the crystal follow exactly the same line as in the special case considered in the last section. Equations (13), (14), and (16) are essentially unchanged:

$$\langle q_1, q_2, \cdots\rangle_{Av}=\xi\mu_1^{q_1}\mu_2^{q_2}\cdots\exp\left[-\chi/kT\right], \tag{31}$$

$$\phi=\sum_q \xi\mu_1^{q_1}\mu_2^{q_2}\cdots\exp\left[-\chi/kT\right],$$

$$\xi\frac{\partial\phi}{\partial\xi}=N_1, \quad \mu_i\frac{\partial\phi}{\partial\mu_i}=N_1w, \tag{32}$$

and

$$(\mu_i)_{T=\infty}=\frac{w}{1-w}. \tag{33}$$

But now the total number of pairs in the whole set of groups is $N_1\gamma$ while the total number of pairs of nearest neighbors in the actual crystal is N_1z. Hence the energy expression (12) should be modified by multiplying the right-hand side with a factor z/γ. Thus we have, in place of (17),

$$\bar{E}=-\frac{z}{\gamma}\sum_q\langle q_1, q_2, \cdots\rangle_{Av}\chi(q_1, q_2, \cdots) =\frac{z}{\gamma}kT^2\frac{\partial\phi}{\partial T}. \tag{34}$$

And (22) becomes, with the help of (3), (20), and (33),

$$F(w,T)=-\frac{z}{\gamma}N_1kT\left[\log N_1+\left(a+b-\frac{2\gamma}{z}\right) \times\{(1-w)\log(1-w)+w\log w\} -\log\xi-w\sum_i\log\mu_i\right]. \tag{35}$$

Differentiate (35) and we obtain

$$\frac{\partial}{\partial w}F(w, T)$$

$$=\frac{z}{\gamma}N_1kT\log\left[(\prod_i \mu_i)\left(\frac{1-w}{w}\right)^{a+b-(2\gamma/z)}\right], \quad (36)$$

where use has been made of (32). So the condition of equilibrium is given by

$$\prod_i \mu_i=\left(\frac{w}{1-w}\right)^{a+b-(2\gamma/z)}. \quad (37)$$

In actual calculations the following points may prove helpful:

(i) *The free energy is changed by a constant if V_{AA} and V_{BB} are both replaced by $\frac{1}{2}(V_{AA}+V_{BB})-V_{AB}$, and V_{AB} by 0.* To prove this let z_i be the number of sites in the group neighboring to the site i. Let χ be changed into χ' by the replacement. It is evident that $\chi'-\chi=-\gamma V_{AB}+$(No. of BB pairs)$(V_{AA}-V_{BB}/2)+$(No. of AA pairs) $\times(V_{BB}-V_{AA}/2)$, and that

$$\sum_{\alpha\text{-sites}} q_iz_i-\sum_{\beta\text{-sites}} q_iz_i$$
$$=\text{(No. of } BB \text{ pairs)}-\text{(No. of } AA \text{ pairs)}. \quad (38)$$

Hence

$$\langle q_1, q_2, \cdots\rangle_{Av}=\xi\mu_1^{q_1}\mu_2^{q_2}\cdots\exp\left[-\chi/kT\right]$$
$$=\xi'\mu_1'^{q_1}\mu_2'^{q_2}\cdots\exp\left[-\chi'/kT\right],$$

if we put

$$\xi'=\xi\exp\left[-\gamma V_{AB}/kT\right],$$
$$\mu_i'=\mu_i\exp\left[\pm z_i(V_{AA}-V_{BB})/2kT\right]$$

where the + sign or the − sign is to be taken according as the site i is an α-site or a β-site. We can now calculate the new free energy and verify the above statement.

(ii) *Sites that are symmetrically situated in the group have μ's equal irrespective of their nature if $V_{AA}=V_{BB}$ and $V_{AB}=0$.* This has already been shown in the last section for the special case considered there. With allowances for change of notation, the proof holds in general. Since the most troublesome part of the calculations is the elimination of the parameters, much might be gained by choosing a group with a large number of sites symmetrically situated.

(iii) *The free energy is a function of s^2, so that (37) is always satisfied at $w=\frac{1}{2}$ (i.e., long-distance order $=0$).* The proof is simple when we have already made $V_{AA}=V_{BB}$ and $V_{AB}=0$, so that an interchange of A and B atoms does not alter the energy:

$$\chi(q_1, q_2, \cdots)=\chi(1-q_1, 1-q_2, \cdots).$$

For, putting

$$\xi'=\xi\mu_1\mu_2\cdots$$

and

$$\mu_i'=1/\mu_i, \quad (39)$$

we get

$$\xi\mu_1^{q_1}\mu_2^{q_2}\cdots\exp\left[-\chi/kT\right]$$
$$=\xi'\mu_1'^{1-q_1}\mu_2'^{1-q_2}\cdots\exp\left[-\chi/kT\right].$$

Thus if (32) is satisfied

$$\sum_q (1-q_i)\xi'\mu_1'^{1-q_1}\mu_2'^{1-q_2}\cdots\exp\left[-\chi/kT\right]$$
$$=\sum_q \xi\mu_1^{q_1}\mu_2^{q_2}\cdots\exp\left[-\chi/kT\right]$$
$$-\sum_q q_i\xi\mu_1^{q_1}\mu_2^{q_2}\cdots\exp\left[-\chi/kT\right]=N(1-w);$$

i.e., ξ', μ_1', μ_2', $\cdots$ would be the solution of (32) with $(1-w)$ substituted for w. Hence by (32) and (20)

$$\Psi(1-w, T)=N_1-N_1\log\xi'$$
$$-\sum_i N_1(1-w)\log\mu_i'=\Psi(w, T)$$

showing that

$$F(w, T)=F(1-w, T). \quad (40)$$

(iv) *The parameter for a corner site is always given by:*

$$\epsilon=\frac{1}{1+s}\{[x^2s^2+(1-s^2)]^{\frac{1}{2}}-sx\} \quad (41)$$

where x is given by (27) and $s=1-2w$, irrespective of the size of the group, if $V_{AA}=V_{BB}$, $V_{AB}=0$. By a corner site is meant a site that has only one nearest neighbor in the group. Let ϵ be the selective variable (parameter) of a corner site, and μ_1 that of its only neighbor in the group. If the corner site is dropped, a new group is obtained. We distinguish all quantities referring to this new group by a prime, and obtain at

once

$$\xi'\frac{\partial\phi'}{\partial\xi'}=N_1,\quad \mu_i'\frac{\partial\phi'}{\partial\mu_i'}=N_1w,\quad i=1,2,\cdots. \tag{42}$$

The sites of the primed group are numbered in the same way as in the unprimed group. Introducing the variable x defined in (27) we may write

$$\begin{aligned}\phi&=\sum_q \xi\mu_1^{q_1}\mu_2^{q_2}\cdots\exp\left[-\chi/kT\right]\\&=\sum_{q_2\cdots}\xi(1+\epsilon x)\mu_2^{q_2}\mu_3^{q_3}\cdots\exp\left[-\chi'/kT\right]\\&\quad+\mu_1\sum_{q_2\cdots}\xi(\epsilon+x)\mu_2^{q_2}\cdots\exp\left[-\chi'/kT\right].\end{aligned} \tag{43}$$

Let these two terms be denoted by ϕ_0 and ϕ_1, respectively. Since

$$\phi=N_1,\quad \mu_1\frac{\partial\phi}{\partial\mu_1}=N_1w,$$

we have

$$\phi_0=N_1(1-w),\quad \phi_1=N_1w. \tag{44}$$

Now

$$\epsilon\frac{\partial\phi_0}{\partial\epsilon}=\frac{\epsilon x}{1+\epsilon x}\phi_0,\quad \epsilon\frac{\partial\phi_1}{\partial\epsilon}=\frac{\epsilon}{\epsilon+x}\phi_1.$$

Hence $\epsilon\dfrac{\partial\phi}{\partial\epsilon}=N_1w$ leads to

$$\frac{\epsilon x}{1+\epsilon x}N_1(1-w)+\frac{\epsilon}{\epsilon+x}N_1w=N_1w, \tag{45}$$

or

$$\frac{w}{1-w}=\frac{\epsilon(\epsilon+x)}{1+\epsilon x}, \tag{46}$$

the solution of which is (41). Thus the two parameters μ and ν in the approximation discussed in Section 2 are all equal to ϵ.

(v) *The contribution to the free energy from a corner atom is such that, in the notation of* (iv)

$$F(w,T)=\frac{\gamma-1}{\gamma}F'(w,T)+\frac{1}{\gamma}F_0(w,T), \tag{47}$$

where $F_0(w,T)$ is the free energy obtained when $\gamma=1$, i.e., *the free energy (9) for the approximation discussed in Section 2.* This is proved as follows. If we put

$$\xi=\xi''\frac{1}{1+\epsilon x},\quad \mu_1=\mu_1''\frac{1+\epsilon x}{\epsilon+x},\quad \mu_i=\mu_i'',\quad i\geqq 2, \tag{48}$$

it is evident from (43) that ϕ would become a function of ξ'', μ_1'', μ_2'', $\cdots$ satisfying the relations

$$\xi''\frac{\partial\phi}{\partial\xi''}\left(=\xi\frac{\partial\phi}{\partial\xi}\right)=N_1,\quad \mu_i''\frac{\partial\phi}{\partial\mu_i''}\left(=\mu_i\frac{\partial\phi}{\partial\mu_i}\right)=N_1w,$$
$$i=1,2,\cdots. \tag{49}$$

It is also evident that ϕ is the same function of ξ'', μ_1'', μ_2'', $\cdots$ as ϕ' is of ξ', μ_1', μ_2'', $\cdots$. Now (42) has only one[8] set of solutions in ξ' and μ_i'. Hence from (49) we infer that $\xi'=\xi''$, and $\mu_i'=\mu_i''$. Thus

$$\xi=\frac{\xi'}{1+\epsilon x},\quad \mu_1=\mu_1'\frac{1+\epsilon x}{\epsilon+x},\quad \mu_i=\mu_i',\quad i\geqq 2. \tag{50}$$

(41) and (50) give the parameters μ_i in terms of μ_i'. Inserting them into (35) we obtain

$$\begin{aligned}F(w,T)&=-N_1kT\frac{z}{\gamma}\Big[\log N_1+\left(a+b-\frac{2\gamma}{z}\right)\\&\quad\times\{(1-w)\log(1-w)+w\log w\}\\&\quad-\log\xi'+(1-w)\log(1+\epsilon x)\\&\quad+w\log(\epsilon+x)-w\log\epsilon-w\sum_i\log\mu_i'\Big]\\&=\frac{\gamma-1}{\gamma}F'(w,T)-N_1kT\frac{z}{\gamma}\Big[\left(1-\frac{2}{z}\right)\\&\quad\times\{(1-w)\log(1-w)+w\log w\}\\&\quad+(1-w)\log(1+\epsilon x)+w\log\frac{\epsilon+x}{\epsilon}\Big].\end{aligned} \tag{51}$$

If the original group (unprimed) is a pair of neighboring sites, we have $\gamma=1$, and (51) reduces to Eq. (9), i.e., to the free energy in the approximation discussed in Section 2:

$$\begin{aligned}F_0(w,T)&=-zN_1kT\Big[\left(1-\frac{2}{z}\right)\\&\quad\times\{(1-w)\log(1-w)+w\log w\}\\&\quad+(1-w)\log(1+\epsilon x)w\log\frac{\epsilon+x}{\epsilon}\Big].\end{aligned} \tag{52}$$

Inserting (52) back into (51) we get (47).

5. COMPARISON WITH BETHE'S METHOD

Both the quasi-chemical method and Bethe's method start from some assumption regarding the relative probabilities of finding a definite group of sites occupied in different ways by atoms. Although in the two methods the arguments leading to the assumptions are in no way similar the assumptions themselves are closely related. In fact, a comparison of Bethe's local partition function and our function ϕ shows that the quasi-chemical method would give the same probabilities of occurrence of the local configurations as Bethe's method if the free energy (35) has a minimum when

$$(\mu)_{\text{interior sites}}=1, \tag{53}$$

i.e., if (37) and (53) are mathematically equivalent. This is not true in general. But it holds approximately when the group of sites under consideration becomes very large. For then,

$$a+b-\frac{2\gamma}{z}\ll\gamma,$$

hence if (53) is true, we should have

$$\left[(\prod_i \mu_i)\left(\frac{1-w}{w}\right)^{a+b-(2\gamma/z)}\right]^{1/\gamma}$$

$$\leqq[\prod(\mu)_{\text{interior sites}}]^{1/\gamma}\leqq 1,$$

so that by (37)

$$\frac{\partial}{\partial w}F(w, T)\leqq 0.$$

To see how the equilibrium free energy $\bar{F}(\bar{w}, T)$ varies with T in high order approximations, we substitute (37) into (35) and obtain by making use of (32)

$$-\frac{F}{zN_1kT}=\frac{1}{\gamma}\log\left(\sum_q \mu_1^{q_1}\mu_2^{q_2}\cdots\exp\left[-\chi/kT\right]\right)$$

$$+\frac{1}{\gamma}\left(a+b-\frac{2\gamma}{z}\right)\log(1-\bar{w}).$$

The last term is very small for large groups, so that by (53)

$$-\frac{F}{zN_1kT}=\frac{1}{\gamma}\log\left(\sum\exp\left[-\chi/kT\right]\right).$$

This shows that in high order approximations the free energy in the quasi-chemical method reduces to the exact form demanded by statistical mechanics.

Recently a modification of Bethe's method has been developed by Wang.[9] This modified Bethe's method bears a very close relation to the quasi-chemical method. The difference between the two lies in the calculation of energy which is discussed in length in Wang's paper.

6. THE NON-INTERFERENCE OF LOCAL CONFIGURATIONS

Let us return to the fundamental assumption of the quasi-chemical method, i.e., to (31) which gives the average numbers of the different local configurations (so far called groups) in the crystal. This equation expresses the exact distribution law of an assembly of molecules (cf. the example in Section 2) which has an energy γ/z times as large as the crystal. Distinguishing all quantities referring to the assembly of molecules by a subscript m, we get from (4),

$$\frac{1}{kT}F(w, T)+\log g(w)$$

$$=\frac{z}{\gamma}\left[\frac{1}{kT}F_m(w, T)+\log g_m(w)\right].$$

But if H is the number of arrangements in the crystal lattice having the given values of $[q_1, q_2, \cdots]$,

$$F(w, T)=-kT\log(\bar{H})+\bar{E}. \tag{54}$$

Thus

$$\log\frac{\bar{H}}{g(w)}=\frac{z}{\gamma}\log\frac{\bar{H}_m}{g_m(w)}. \tag{55}$$

But*

$$H_m=\frac{N_1!}{\prod_q[q_1, q_2, \cdots]!}.$$

On substituting this into (55) and dropping the bars we get

$$H=h(w)\left\{\frac{N_1!}{\prod_q[q_1, q_2, \cdots]!}\right\}^{z/\gamma}, \tag{56}$$

---

[9] J. S. Wang, "Approximate partition function in generalized Bethe's theory of superlattices" (to be published).

* R. H. Fowler, *Statistical Mechanics*, second edition, 2.6 and 5.11.

where

$$h(w)=g(w)/\{g_m(w)\}^{z/\gamma}. \tag{57}$$

Equation (56) has been referred to in Fowler and Guggenheim's paper[1] as the mathematical expression of the "hypothesis of the non-interference of local configurations (pairs);" because when $z/\gamma=1$, the number of arrangements in the crystal consistent with the distribution law $[q_1, q_2, \cdots]$ for the groups of sites is, except for the factor $h(r)$, equal to

$$H_m=\frac{N_1!}{\prod_q [q_1, q_2, \cdots]!},$$

which would be the number of arrangements in the crystal having the given values of $[q_1, q_2, \cdots]$ if the N_1 groups in the crystal were *separated* and were filled *independently* with atoms. The term "non-interference" comes from the fact that the N_1 groups are *not separated* but are *interlocked* and *cannot be filled independently* with atoms, i.e., they "interfere" with each other.

To find the value of $g(w)$ we notice that by definition $g_m=\Sigma H_m$. But ΣH_m is the number of arrangements in the *separated* groups considered above if they are to be so filled with atoms that N_1w of them have wrong atoms on the sites i, where $i=1, 2, \cdots$. For the N_1 sites i of the N_1 groups,

$$\frac{N_1!}{\{N_1(1-w)\}!(N_1w)!}$$

different arrangements are possible. Hence

$$g_m=\sum H_m=\sum\frac{N_1!}{\prod_q [q_1, q_2, \cdots]!}$$

$$=\left[\frac{N_1!}{\{(1-w)N_1\}!(N_1w)!}\right]^{a+b}. \tag{58}$$

Thus

$$h(w)=\left[\frac{N_1!}{\{N_1(1-w)\}!(N_1w)!}\right]^{2-(z/\gamma)(a+b)}. \tag{59}$$

The free energy of the crystal may be obtained from (40), (42), and (45) as:

$$F(w, T)=\bar{E}-\frac{zN_1kT}{\gamma}\left\{\left(a+b-\frac{2\gamma}{z}\right)\right.$$

$$\times[(1-w)\log(1-w)+w\log w]+\log N_1$$

$$\left.-\sum_q\frac{1}{N_1}\langle q_1, q_2, \cdots\rangle_{Nw}\log\langle q_1, q_2, \cdots\rangle_{Nw}\right\},$$

which is reducible to Eq. (35) obtained above.

7. SPECIAL CONSIDERATIONS CONCERNING BETHE'S FIRST AND SECOND APPROXIMATIONS

The First Approximation

If an α-site together with its z nearest neighbors are taken as our group of interest, all the sites except the central one are corner sites. Hence their selective variables are all equal to the value of ϵ given in (41). By successive applications of (47) we see that the free energy is exactly $F_0(w, T)$, a fact which has already been pointed by Fowler and Guggenheim.[1] The selective variable of the central site is given by successive applications of (50):

$$\lambda=\frac{w}{1-w}\left(\frac{1+\epsilon x}{\epsilon+x}\right)^z. \tag{60}$$

The factor $w/(1-w)$ is the selective variable of the central site when it alone forms the group. The equilibrium condition (38) becomes

$$\lambda\epsilon^z=[\bar{w}/(1-\bar{w})]^{z-1}. \tag{61}$$

But by (60) and (45)

$$\lambda=[w/(1-w)]^{1-z}\epsilon^z.$$

Hence at equilibrium

$$\lambda=1. \tag{62}$$

Thus the approximation is completely equivalent to Bethe's first approximation, as already mentioned in Section 5.

The Second Approximation

Now consider the group of sites occurring in Bethe's second approximation. According to Section 4 (iv), the selective variables for the corner sites in the second shell are all equal to the parameter ϵ given by (41). In Bethe's original calcula-

tions, however, the selective variables for the corner sites and the medium sites are made equal, and are found to be different from ϵ. Thus if we use his original method, Eq. (32) would not be satisfied. In other words, the probabilities of occurrence of wrong atoms in the corner and medium sites would be unequal.

For simplicity we shall drop the corner sites and take as our group of interest the central site, the first shell sites and the medium sites with selective variables μ, ν, and λ, respectively. The contribution by the corner sites can be included in the free energy by simple addition, as shown in Section 4. With the notations n and g_{nm} of Bethe[3] we find

$$\phi=\xi\sum_n (x^n+\mu x^{z-n})P_n(x,\nu,\lambda), \qquad (63)$$

where

$$P_n(x,\nu,\lambda)=\nu^n\sum_m g_{nm}[(1+\lambda)x]^m \times(x^2+\lambda)^{([z/2]-1)n-(m/2)}(1+\lambda x^2)^{([z/2]-1)(z-n)-(m/2)}.$$

After the elimination of ξ and μ, (32) becomes

$$zw=\frac{\sum_{l,n}\left\{2x^{l+z-n}\left[(1-w)P_n\lambda\frac{\partial}{\partial\lambda}P_l+wP_l\lambda\frac{\partial}{\partial\lambda}P_n\right]\right\}}{(z-2)(\sum_n x^nP_n)(\sum_n x^{z-n}P_n)}$$

$$=\frac{\sum_{l,n}\left\{x^{l+z-n}\left[(1-w)P_n\nu\frac{\partial}{\partial\nu}P_l+wP_l\nu\frac{\partial}{\partial\nu}P_n\right]\right\}}{(\sum_n x^nP_n)(\sum_n x^{z-n}P_n)}. \qquad (64)$$

The free energy is obtained from (35):

$$F(w,T)=-\frac{N_1kT}{z-1}\Big[\tfrac{1}{2}(z^2-4z+4) \times\{(1-w)\log(1-w)+w\log w\} +(1-w)\log(\sum_n x^nP_n) +w\log(\sum_n x^{z-n}P_n)-zw\log\nu -w\frac{z(z-2)}{2}\log\lambda\Big]. \qquad (65)$$

8. APPLICATION TO THE CRYSTAL Cu_3Au

For the face-centered crystal Cu_3Au, we may of course follow Peierls[10] and take as our group of interest a central site together with its twelve first shell neighbors. The free energy expression would then contain seven selective variables, four of which may be easily eliminated. The resulting expression is very cumbersome and numerical calculations would be laborious. We therefore make a simpler approximation: The group is taken to be four nearest neighbors forming a tetrahedron. (See Fig. 2.) A little

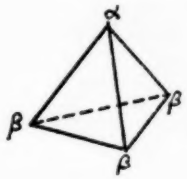

FIG. 2.

geometrical consideration assures us that all such tetrahedrons contain an α-site (for gold atoms) and three β-sites (for copper atoms), an interesting conclusion showing that the tetrahedron might be regarded as a sort of "molecular" structure in a faced-centered lattice with atomic ratio 1:3. Our approximation may thus be reasonably expected to reveal the more important features of the order-disorder transformation in such alloys.

A little reflection shows that the statement made in Section 4 (i) still holds, so that we may put $V_{AA}=V_{BB}$ and $V_{AB}=0$. Let μ and ν be the parameters (for the wrong atoms) of the β-sites and the α-sites, respectively. Let there be altogether $N=4N_1$ atoms. It is easy to see that there are $8N_1$ groups in the crystal. When N_1w atoms on the α-sites are wrong, the equations determining the parameters are

$$8N_1=\phi=\xi[x^3+3x^2\mu+3x^3\mu^2+x^6\mu^3 +\nu(x^6+3x^3\mu+3x^2\mu^2+x^3\mu^3)], \qquad (66a)$$

$$8N_1w=\nu\frac{\partial\phi}{\partial\nu}=\xi\nu(x^6+3x^3\mu+3x^2\mu^2+x^3\mu^3), \qquad (66b)$$

and

$$8N_1\left(\frac{w}{3}\right)+8N_1\left(\frac{w}{3}\right)+8N_1\left(\frac{w}{3}\right)=\mu\frac{\partial\phi}{\partial\mu} =3x^2\xi\mu[1+2x\mu+x^4\mu^2+\nu(x+2\mu+x\mu^2)], \qquad (66c)$$

where x is defined by (27). The energy of the

[10] R. Peierls, Proc. Roy. Soc. **A154**, 207 (1936).

crystal is [cf. (34)],

$$\bar{E}=\tfrac{1}{2}kT^2\frac{\partial\phi}{\partial T}+\text{constant}; \qquad (67)$$

so that the free energy becomes [cf. (35)]:

$$F(w,T)=-kT[\log g(w)+\tfrac{1}{2}(\phi-8N_1\log\xi -8N_1w\log\nu-8N_1w\log\mu)_{T=\infty}].$$

But

$$\log g(w)=-N_1\Big[(1-w)\log(1-w)+w\log w +w\log\frac{w}{3}+(3-w)\log\{(3-w)/3\}\Big],$$

and at $T=\infty$,

$$\nu=\frac{w}{1-w},\quad \mu=\frac{w}{3-w},\quad \xi=8N_1(1-w)\left(1-\frac{w}{3}\right)^3.$$

Hence

$$-\frac{F(w,T)}{N_1kT}=-9\log 3+4\log(8N_1) +6w\log w+3(1-w)\log(1-w) +3(3-w)\cdot\log(3-w)-4\log\xi -4w\log\mu-4w\log\nu. \qquad (68)$$

Since ξ and ν can be very easily solved from (66), numerical calculations are quite simple. The value of the free energy is plotted in the accompanying figure (Fig. 3).

The equilibrium value of w is given by [cf. (36) and (37)]:

$$0=-3\log\frac{(1-\bar{w})(3-\bar{w})}{\bar{w}^2}+4\log\mu\nu. \qquad (69)$$

This is always satisfied at $w=\frac{3}{4}$.* Actual calculation shows that the absolute minimum of the free energy is or is not at $w=\frac{3}{4}$ according as $x>0.2965$ or $x<0.2965$. From the form of the curve in Fig. 3 it is seen that the crystal has a critical temperature at which the long-distance order, and hence also the energy, is discontinuous. The critical temperature T_c and the latent heat Q are found to be given by

$$T_c=0.8228\frac{1}{k}[\tfrac{1}{2}(V_{AA}+V_{BB})-V_{AB}],$$

and

$$Q=0.8824N_1[\tfrac{1}{2}(V_{AA}+V_{BB})-V_{AB}].$$

In terms of the total energy change from $T=0$ to $T=\infty$:

$$E_0=3N_1[\tfrac{1}{2}(V_{AA}+V_{BB})-V_{AB}],$$

these quantities become, with the usual notation

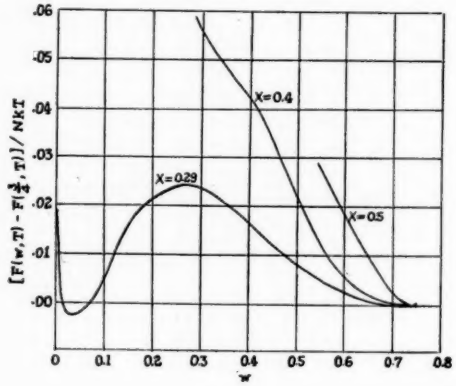

FIG. 3.

$$R=4N_1k,$$

$$T_c=1.097E_0/R,\quad\text{and}\quad Q=0.2941E_0.$$

In Bragg and Williams' approximation, they are given by

$$T_c=2.19E_0/R,\quad\text{and}\quad Q=0.218E_0;$$

and in Peierls' approximation,[10] they are given by

$$T_c\leqq 1.3E_0/R,\quad\text{and}\quad Q\leqq 0.36E_0.$$

It will be noticed that because of the lack of a free energy expression Peierls did not give the exact values of these quantities.

In conclusion the author wishes to express his thanks to Professor J. S. Wang for valuable criticism and advice.

* This is not evident from (69) directly. But if we divide the whole crystal into four simple cubic sublattices and introduce a w for each sublattice so that Nw is the number of A atoms on the jth sublattice, $j=1, 2, 3, 4$, it is obvious that the free energy is symmetrical in the w's. From this we infer that (69) is satisfied at $w=\frac{3}{4}$.

THE JOURNAL OF CHEMICAL PHYSICS VOLUME 13, NUMBER 2 FEBRUARY, 1945

Statistical Thermodynamics of High-Polymer Solutions

I. Theory for Dilute Solutions

TURNER ALFREY AND PAUL DOTY
Department of Chemistry, Polytechnic Institute of Brooklyn, Brooklyn, New York
(Received November 17, 1944)

Previous theoretical treatments of the thermodynamics of high-polymer solutions have assumed that the entropy of mixing is independent of the magnitude of the heat of mixing. The present treatment considers energy interactions on a molecular scale and includes these in the configurational partition function. This leads to the derivation of expressions for the heat of mixing and the entropy of mixing which reflect the effect of solvent-solute interaction. One result of particular interest is an explicit expression for the temperature dependence of osmotic pressure.

INTRODUCTION

SOLUTIONS of high-polymer molecules in ordinary organic solvents exhibit such enormous negative deviations from Raoult's law and such peculiar behavior with respect to osmotic pressure that they hold a unique position in the thermodynamics of binary systems.

In an ideal solution, the heat of mixing is zero and the entropy of mixing is given by:

$$\Delta S_{\text{mix}} = -R \sum_i n_i \ln X_i \qquad (1)$$

where n_i is the number of moles and X_i is the mole fraction of the ith component of the solution. The partial molal entropy of mixing of the solvent, $\Delta\bar{S}_1$, is given by:

$$\Delta\bar{S}_1 = -R \ln X_1,$$

which is obtained from the partial differentiation of (1) with respect to n_1.

These relationships can be derived by means of statistical mechanics if one adopts the following molecular picture of a binary mixture containing N_A molecules of the type A and N_B molecules of the type B.

1. A given molecular arrangement of the mixture can be adequately described by specifying the occupants of all lattice sites in a quasi-lattice of (N_A+N_B) sites. The total energy of the mixture can be unambiguously divided into two parts—one of which (independent of the molecular arrangement in the mixture) is simply equal to the energy of the separated components, and one of which (the "configuration" energy) depends upon the pattern of the molecular arrangement. Thus the partition function for the mixture can be factored into the partition functions for the two separated components and a configurational partition function which determines the free energy of mixing.

2. The configurational energy to a satisfactory approximation can be expressed as the sum of interaction energies of nearest neighbor pairs of site-occupants.

3. The contribution of an A-B pair to the configurational energy is simply the arithmetic mean of the contributions of an A-A pair and a B-B pair, respectively; i.e., $\epsilon_{AB}=(\epsilon_{AA}+\epsilon_{BB})/2$. It follows that all arrangements of molecules in the lattice represent the same energy, and hence the configurational partition function reduces to a simple counting of all the possible modes of packing the two kinds of molecules into the lattice.

4. The two molecules are of roughly the same size and shape, so that a given site of the lattice will be occupied by either exactly one A molecule or exactly one B molecule.

Deviations from the laws of ideal solutions,[1] in the case of organic compounds, are generally attributed to failure of assumption (3) or (4) rather than of assumptions (1) and (2).

If $\epsilon_{AB}\neq(\epsilon_{AA}+\epsilon_{BB})/2$, the heat of solution will not be zero. Furthermore, a rigorous statistical mechanical treatment indicates that failure of assumption (3) will also change the *entropy* of mixing from the value given in Eq. (1). This

[1] R. H. Fowler and E. A. Guggenheim, *Statistical Thermodynamics* (University Press, Cambridge, England, 1939), p. 351.

latter effect, however, is secondary in importance to the introduction of a non-zero heat of mixing. Indeed, Hildebrand and others have shown that the retention of the classical *entropy* of mixing even in the presence of a non-zero heat of mixing often represents (for mixtures of molecules of about the same size and shape) a very useful approximation. Mixtures for which this approximation is justified have been called "regular."

A different type of deviation from Raoult's law occurs when assumption (3) applies but assumption (4) fails. Fowler and Rushbrooke,[2] and Chang[3,4] treated the case of a solution of double sized molecules in a solvent of spherical molecules. In such a case, where one solute molecule occupies more than one lattice site of the mixture, the entropy of solution deviates from Eq. (1). The heat of mixing, however, is zero. Such solutions are designated as "athermal."

Athermal solutions of *high polymers* in low molecular weight solvents exhibit extremely large entropy deviations of this type. Meyer[5] discussed the problem qualitatively on the basis of a quasi-solid lattice, the cells of which may be occupied by either a solvent molecule or a segment of the polymer molecule. Huggins[6] has extended the work of Fowler and Rushbrooke in a somewhat quantitative manner to polymer solutions. Flory[7] using Meyer's model has arrived at practically an identical expression for the entropy of mixing. Miller[8] has improved upon the analyses of Chang by applying the Bethe approximation to evaluate the entropy of mixing of solvent molecules with "polymers" of two and three units similar in size to the solvent. By a consideration of the way in which the results depended upon the number of units he made an extrapolation to very long polymer molecules. The expressions for osmotic pressure, vapor pressure, and other thermodynamic properties given by these quantitative theories are in substantial agreement with the general behavior of high-polymer solutions.

Flory and Huggins have extended their theories to the more general problem of a high-polymer solution with a non-zero heat of mixing by an approximation similar to that used by Hildebrand[9] and Scatchard[10] in the case of low molecular weight liquids.

For an approximation to the entropy of mixing in the general case, they use the expression derived for the athermal case and further assume that the partial molal heat of solution of the solvent is proportional to the square of the solute concentration (which must be true for low concentrations). They suggest for the partial molal free energy of solution the expression:

$$\Delta\bar{F}_1=\Delta\bar{H}_1-T\Delta\bar{S}_1=kc^2-T\Delta\bar{S}_1 \text{ (athermal)}. \quad (2)$$

In this present state of the thermodynamic theory of high-polymer solutions two aspects are inadequately treated. First, the entropy of mixing is calculated for the case where the heat of mixing is zero, and this value is then used for real solutions where there is a considerable heat of mixing. It is well recognized that this is not rigorously correct, since the presence of a heat of mixing must necessarily reflect a fundamental difference in energy among different configurations and hence a certain amount of intermolecular clustering.* Such clustering will result in a change of the entropy of mixing from that calculated for the case of zero heat of mixing. Second, no adequate provision for the temperature dependence of the osmotic pressure, vapor pressure, and other thermodynamic properties is included in the present theories.

In this paper, the energy differences among configurations are taken into account at an earlier stage of the treatment, i.e., in the calculation of the partition function itself. This permits the following treatment of the above-mentioned points.

THE CONFIGURATIONAL PARTITION FUNCTION

The model used here to represent a high-polymer solution is the simplest that is com-

[2] R. H. Fowler and G. S. Rushbrooke, Trans. Faraday Soc. **33**, 1272 (1937).
[3] T. S. Chang, Proc. Camb. Phil. Soc. **35**, 293 (1939).
[4] T. S. Chang, Proc. Roy. Soc. **A169**, 512 (1939).
[5] K. H. Meyer, Zeits. f. physik. Chemie **B44**, 383 (1939).
[6] M. L. Huggins, J. Phys. Chem. **46**, 151 (1942).
[7] P. J. Flory, J. Chem. Phys. **10**, 51 (1942).
[8] A. R. Miller, Proc. Camb. Phil. Soc. **39**, 54 (1942).
[9] J. H. Hildebrand, Chem. Rev. **18**, 315 (1935).
[10] G. Scatchard, Chem. Rev. **8**, 321 (1931).
*By "clustering" is meant any non-random distribution among configurations. This will include both deviations toward clusters of similar species (to be expected in cases of endothermic mixing) and deviations toward a regular "checkerboard" structure (to be expected in cases of exothermic mixing).

patible with the present conception of these solutions. The configurations in these solutions are considered to be represented by a quasi-crystalline lattice of n_0 sites, which can be alternatively occupied by a solvent molecule or a segment of a polymer molecule. This lattice contains n_2 polymer molecules each composed of p segments and $(n_0-pn_2)=n_1$ solvent molecules. Our problem is to obtain the configurational partition function for such an assembly where interaction of the components results in a non-random distribution among configurations. The coordination number of the lattice is denoted by γ.

Provided that the internal degrees of freedom can be separated from the configurational degrees of freedom, the configurational partition function, Ω, is given by

$$\Omega=\sum_{\substack{\text{over all}\\ \text{configurations}}} e^{-E_c/kT}\equiv\sum_{E_c} g_{E_c}e^{-E_c/kT}, \quad (3)$$

where g is the degeneracy and E_c is the configurational potential energy made up as follows:

$$E_c=M_{11}\epsilon_{11}+M_{12}\epsilon_{12}+M_{22}\epsilon_{22}. \quad (4)$$

Here, ϵ_{11}, ϵ_{12}, and ϵ_{22} are the mutual potential energies of pairs of solvent, solvent-solute, and solute molecules, respectively, and the M's are the corresponding numbers of such pairs. It is clear that $\gamma n_1=2M_{11}+M_{12}$ and that $(\gamma-2)pn_2=2M_{22}+M_{12}$. In view of these linear relationships between M_{11}, M_{12}, and M_{22}, E_c may be written simply as:

$$E_c=E_0'+M_{12}\epsilon', \quad (5)$$

where $E_0'=\frac{1}{2}[\gamma n_1\epsilon_{11}+(\gamma-2)pn_2\epsilon_{22}]$—i.e., the energy of the separated components—and ϵ' is $[\epsilon_{12}-(\epsilon_{11}+\epsilon_{22})/2]$. This can alternatively be written as:

$$E_c=E_0+M_{22}\epsilon, \quad (6)$$

where E_0, the energy of a hypothetical mixture in which there are no 2-2 nearest neighbors pairs, is defined as

$$\tfrac{1}{2}[\gamma n_1-(\gamma-2)pn_2]\epsilon_{11}+(\gamma-2)pn_2\epsilon_{12},$$

and ϵ as

$$\epsilon_{11}+\epsilon_{22}-2\epsilon_{12}.$$

The direct evaluation of Ω using (4) would be prohibitively complicated, but the use of Eq. (6) for the configurational potential energy permits the following solution of the problem.

Let us return to the model, where γ is the coordination number of the lattice. If x polymer molecules have already been located in this lattice and we are considering the number of ways of placing the $(x+1)$th polymer molecule, we may distinguish three types of lattice sites: (1) Those sites which are already occupied. (2) Those sites which are unoccupied, but are adjacent to occupied sites. (3) Sites surrounded only by unoccupied sites.

The number of sites of the first type is obviously equal to px. We introduce the approximation that the number of sites of type 2 is given by $px(\gamma-2)$. We thus picture each polymer molecule as being surrounded by an envelope of adjacent sites, $p(\gamma-2)$ in number, and assume that the total number of sites adjacent to polymer molecules is given by the sum of these individual envelopes. This will not be justified at high concentration, where the envelopes of different polymer molecules will interpenetrate. When such interpenetration becomes significant, our expression will overcount the number of sites of type 2. To the approximation that $px(\gamma-2)$ gives the number of sites of type 2, the remaining number of sites (type 3) will be given by $n_0-px(\gamma-1)$. If there is solvent-solute interaction, the availability of sites of type 2 is to be weighted by a factor $e^{-\epsilon/kT}$ which will make the occupation of these sites more or less probable according to the type of interaction present. The need for defining E_c by Eq. (6) now becomes apparent, for the availability of type 2 sites must be characterized by a single energy parameter in this model.

The complexions* available for the $(x+1)$th polymer molecule are counted by considering first the addition of the terminal segment followed by successive segments. The number of available sites for this terminal segment is

$$n_0-px(\gamma-1)+px(\gamma-2)e^{-\epsilon/kT},$$

and the expected number of available unoccupied sites adjacent to the site occupied by the terminal

* The word complexion is used to mean any geometrically possible configuration weighted according to how many type 2 sites it includes.

segment of this polymer chain will be

$$\gamma\frac{n_0-px(\gamma-1)+px(\gamma-2)e^{-\epsilon/kT}}{n_0}.$$

For the third and successive segments, this quantity, which may be called α, will be

$$\alpha=(\gamma-1)\frac{n_0-px(\gamma-1)+px(\gamma-2)e^{-\epsilon/kT}}{n_0}. \quad (7)$$

The number of complexions available to a chain without shifting its terminal group is

$$\gamma\frac{n_0-px(\gamma-1)+px(\gamma-2)e^{-\epsilon/kT}}{n_0}\alpha^{p-2}, \quad (8)$$

thus the total number of complexions for the chain in the lattice is

$$\psi_{x+1}=\tfrac{1}{2}[n_0-px(\gamma-1)+px(\gamma-2)e^{-\epsilon/kT}]\times\frac{\gamma}{\gamma-1}\alpha^{p-1}, \quad (9)$$

where the factor $\frac{1}{2}$ compensates for the presumed indistinguishability of the two chain ends. To the approximation that $\gamma/\gamma-1=1$, Eq. (9) becomes, after introducing Eq. (7),

$$\psi_{x+1}=\frac{1}{2}\left(\frac{\gamma-1}{n_0}\right)^{p-1}\times[n_0-px(\gamma-1)+px(\gamma-2)e^{-\epsilon/kT}]^p. \quad (10)$$

The configurational partition function may now be expressed as

$$\Omega=\frac{\prod_{x=1}^{n_2}\psi_x}{n_2!}e^{-E_0/kT}. \quad (11)$$

For simplicity the factors $\frac{1}{2}$ and $n!$ in Eqs. (9) and (11) will now be deleted. This is justified since the configurational partition function will be applied only to processes of mixing in which the contributions of these factors are identical for both the initial and final states and hence cancel out.

This partition function can be expanded to yield a polynomial in $e^{-\epsilon/kT}$:

$$\Omega=e^{-E_0/kT}\sum_j\phi_j e^{-j\epsilon/kT}, \quad (12)$$

where ϕ_j is the number of configurations possessing j nearest-neighbor pairs of the type 2-2. Thus the process of counting the possible sites for each successive segment, weighting some sites by the factor $e^{-\epsilon/kT}$ does result in the correct weighting of entire configurations. As given by Eq. (12), Ω is identical to the original definition of Eq. (3). The expanded form (12) will not be used, however.

To evaluate $\Pi\psi_x$, the substitution of Eq. (10) is first made, yielding

$$\left(\frac{\gamma-1}{n_0}\right)^{(p-1)n_2}\times\prod_x[n_0-px(\gamma-1)+px(\gamma-2)e^{-\epsilon/kT}]^p. \quad (13)$$

By defining

$$Y=p(\gamma-1)-p(\gamma-2)e^{-\epsilon/kT}, \quad (14)$$

(13) becomes

$$\left(\frac{\gamma-1}{n_0}\right)^{(p-1)n_2}\prod_x[n_0-Y_x]^p. \quad (15)$$

Let us consider the evaluation of $\ln\Pi[n_0-Yn_2]$, since it is always $\ln\Omega$ that is required for later use. Hence:

$$\ln\prod_x[n_0-Yn_2]^p=\sum_x\ln[n_0-Yn_2]^p=\int_0^{n_2}\ln[n_0-Yx]^p dx$$

$$=p\int_0^{n_2}\ln[n_0-Yx]dx$$

$$=-\frac{p}{Y}\{n_0[\ln(n_0-Yn_2)-\ln n_0]-Yn_2[\ln(n_0-Yn_2)-1]\}. \quad (16)$$

This result may be used to obtain the final form of the configurational partition function after n_0 is replaced by (n_1+pn_2).

$$\ln\Omega=\frac{-E_0}{kT}-\frac{p}{Y}n_1\ln\frac{n_1+pn_2-Yn_2}{n_1+pn_2}+n_2\ln(n_1+pn_2)+(p-1)n_2\ln(\gamma-1)-pn_2+\left(1-\frac{p}{Y}\right)\left(pn_2\ln\frac{n_1+pn_2-Yn_2}{n_1+pn_2}\right). \quad (17)$$

The corresponding $\ln\Omega$ for the two separated components (n_1 molecules of solvent and n_2

molecules of perfectly arranged polymer) is given by $-E_0'/kT$. Hence the free energy of mixing solvent with perfectly arranged polymer is governed by Eq. (17), with E_0 replaced by (E_0-E_0').

To obtain corresponding expressions of the thermodynamic functions for the process of mixing n_1 solvent molecules with n_2 randomly entangled polymer molecules, one should subtract from (17) the sum of terms obtained by putting n_1 equal to zero. That is, for this latter process, the corresponding change in $\ln \Omega$ is given by

$$\ln \Omega' = -\frac{p}{Y} n_1 \ln \frac{n_1+pn_2-Yn_2}{n_1+pn_2} - n_2 \ln \frac{pn_2}{n_1+pn_2} + pn_2\left(1-\frac{p}{Y}\right) \times \left(\ln \frac{n_1+pn_2-Yn_2}{n_1+pn_2} - \ln \frac{pn_2-Yn_2}{pn_2}\right). \quad (18)$$

While this treatment is completely consistent with the fact that individual polymer segments may be in simultaneous contact with more than one other polymer segment, our partition function gradually departs from the true value based on the model at concentrations where the *average* number of neighboring segments exceeds one, (i.e., where $M_{ab} > pn_2/2$), and presumably begins to fail as M_{ab} approaches $pn_2/2$. For moderate values of ϵ, this will occur at a volume fraction of about $1/(\gamma-2)$.

PARTIAL MOLAL QUANTITIES

The partial molal quantities that characterize the thermodynamic behavior of polymer solutions are obtained by differentiating the corresponding thermodynamic quantities for mixing which are in turn obtained from Eq. (18).

For example, the free energy of mixing, ΔF_{mix}, is equal to $RT \ln \Omega'$; that is, Eq. (18) multiplied by RT. When this result is differentiated with respect to n_1, the following expression is obtained for the partial molal free energy of the solvent (free energy of dilution).

$$\Delta \bar{F}_1 = RT\left[\frac{p}{Y} \ln \frac{n_0-Yn_2}{n_0} + \frac{n_2(p-1)}{n_0}\right]. \quad (19)$$

The expression for the partial molal entropy of mixing is obtained from (19) since $-(\partial \Delta \bar{F}_1/\partial T) = \Delta \bar{S}_1$. Thus,

$$\Delta \bar{S}_1 = RT \frac{\partial Y}{\partial T} \frac{p}{Y^2}\left[\frac{Yn_2}{n_0-Yn_2} + \ln \frac{n_0-Yn_2}{n_0}\right] - R\left[\frac{p}{Y} \ln \frac{n_0-Yn_2}{n_0} + \frac{n_2(p-1)}{n_0}\right]. \quad (20)$$

The partial molal heat of mixing is found by substituting the two previous equations into

$$\Delta \bar{H}_1 = \Delta \bar{F}_1 + T\Delta \bar{S}_1, \quad (21)$$

and the result is

$$\Delta \bar{H}_1 = +RT^2 \frac{p}{Y} \frac{\partial Y}{\partial T} \times \left[\frac{1}{Y} \ln \frac{n_0-Yn_2}{n_0} + \frac{n_2}{n_0-Yn_2}\right]. \quad (22)$$

The corresponding quantities for the solute may of course be obtained by differentiating first with respect to n_2 or by the application of the Gibbs-Duhem relation.

DISCUSSION

From a consideration of the statistical effect of solvent-solute interaction on the partition function, the basic equations for the thermodynamics of non-regular high-polymer solutions have been derived. Two illustrations of the use of these equations will be considered here. In another paper we plan to present: (1) experimental confirmation of the present theory; (2) theoretical refinements; and (3) an extension to include solubility and fractionation.

The variation of osmotic pressure with concentration is of vital concern in the determination of molecular weights of high polymers and the slope of the line obtained when π/c is plotted against c, the concentration, is often used as an indication of how "good" or "poor" is the solvent for the polymer. At low concentrations most osmotic pressure data can be represented by an equation of the type

$$\frac{\pi}{c} = A + Bc. \quad (23)$$

By the use of Eq. (19) and the thermodynamic relation, $\pi = -\Delta \bar{F}_1/\bar{V}_1$, where $\bar{V}_1$ is the partial molal volume of solvent, one obtains the follow-

ing equation for the osmotic pressure

$$\pi=\frac{-RT}{V_1}\left[\frac{p}{Y}\ln\frac{n_0-Yn_2}{n_0}+\frac{n_2(p-1)}{n_0}\right]. \quad (24)$$

If this expression is expanded as a power series in concentration, the first two terms yield:

$$\frac{\pi}{c}=\frac{RT}{M}+\frac{RT}{2V_1\rho_2^2}\frac{Y}{p}c,$$

where V_1, the molar volume of solute, replaces $\bar{V}_1$ and ρ_2 is the density of the polymer. If $\epsilon=0$, $Y=p$ and this equation becomes identical with Flory's and similar to Huggins' for osmotic pressure of solutions in which there is no heat of mixing. The plot of Eq. (24) is given in Fig. 1 for such an athermal case (A) where the arbitrary assignments of molecular weight = 100,000, $\rho=0.94$, $V_1=104$ cc, and $T=30$°C have been made. In this graph, osmotic pressure is expressed in units of cm of water. In ideal solutions, van't Hoff's law is obeyed and a horizontal plot is obtained. In athermal polymer solutions, however, the large entropy of mixing gives rise to a very steep slope for the π/c *versus* c plot. This slope is rather insensitive to temperature (varying directly as the absolute temperature).

All measurements* or estimations of heats of mixing for polymer solutions have given only positive values for this quantity. From Eq. (22) it can be seen that this requires the net interaction energy ϵ to be negative. Assigning to ϵ a value of -120 calories and to γ, the coordination number, a value of 6, Eq. (24) gives, for 30°C, the plot labeled C in Fig. 1, the slope of which is of the order magnitude often encountered in actual measurements. With this interaction energy, the slope of the plot has become quite temperature sensitive as is illustrated by plots B and D corresponding to 10° and 50°C, respectively. Thus it is seen that line A represents the osmotic pressure behavior of an "ideal" polymer solution. The further an actual plot is from this line, the larger is the heat of mixing and hence the temperature dependence of its slope. With increasing temperature, its slope changes toward that of line A. The scanty measurements of the temperature dependence of osmotic pressure thus far published and measurements now in progress in this laboratory confirm the general outline just described. It is now obvious that good temperature control is necessary for most measurements of osmotic pressure.

For Fig. 1 to exhibit more quantitative significance it would be necessary to reduce the absolute values of the slopes by introducing, as Flory has done, a correction for the fact that a cell which would enclose an actual segment of a polymer molecule would be filled by several solvent molecules.

As another illustration, one may consider the dependence of the partial molal heat of mixing on concentration. It is this quantity which has heretofore been represented as being proportional to the square of the concentration (10). However,

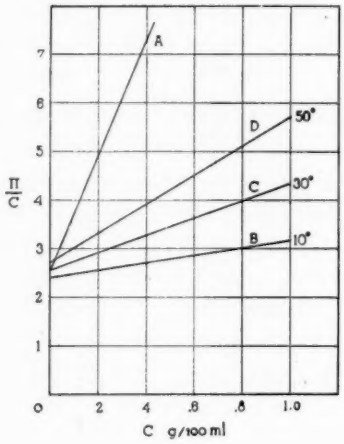

FIG. 1.

Gee and Treloar[11] who have made the only reliable experimental determination of the quantity find that it varies more rapidly than the square of the concentration.

Equation (22) may be transformed as follows:

$$\Delta\bar{H}_1=RT^2\frac{\partial Y}{\partial T}\frac{p}{Y}\left[\frac{n_2/n_0}{1-Y\frac{n_2}{n_0}}+\frac{1}{Y}\ln\left(1-Y\frac{n_2}{n_0}\right)\right]$$

$$=RT^2\frac{\partial Y}{\partial T}\frac{p}{Y}\left[\frac{1}{2}Y\left(\frac{n_2}{n_0}\right)^2+\frac{2}{3}Y^2\left(\frac{n_2}{n_0}\right)^3+\frac{3}{4}Y^3\left(\frac{n_2}{n_0}\right)^4+\cdots\right], \quad (26)$$

* Except the system cellulose triacetate—tetrachloroethane.

[11] G. Gee and L. R. G. Treloar, Trans. Faraday Soc. **38**, 147 (1942).

by expanding and collecting terms. For the choice of constants: $\gamma=6$, $\epsilon=-100$, $V_1=100$, $M=100{,}000$ and $T=300°\text{K}$ this equation reduces to

$$\Delta\bar{H}_1=200[c^2+0.368c^3+0.114c^4+\cdots]. \quad (27)$$

Thus, at the low concentrations where our treatment is valid the square term of the series expansion is dominant. However, in this example, which is far from the extreme case, appreciable contributions from the higher terms appear. This treatment predicts that the $\Delta\bar{H}_1$ will increase with concentration somewhat more rapidly than C^2. This is in agreement with the measurements of $\Delta\bar{H}_1$ by Gee and Trealoar[11] in system rubber-benzene.

An entirely different treatment of this problem by W. C. Orr has just appeared.*

*W. C. Orr, Trans. Faraday Soc. (August, 1944).

THE JOURNAL OF CHEMICAL PHYSICS VOLUME 13, NUMBER 2 FEBRUARY, 1945

The Tetrahedral X_2YZ_2 Molecular Model

Part II. Rotation-Vibration Energies

W. H. SHAFFER
Mendenhall Laboratory of Physics, The Ohio State University, Columbus, Ohio

AND

R. C. HERMAN
Applied Physics Laboratory, Johns Hopkins University, Silver Spring, Maryland

The appropriate quantum-mechanical Hamiltonian is set up according to the method of Wilson and Howard for investigating rotation-vibration energies to second-order approximation. The vibrational term G is derived explicitly as a function of the anharmonic constants, Coriolis parameters, etc. The elements are given for the secular determinant required for evaluation of the rotational term F including dependence on Coriolis interactions, centrifugal stretching, effective moments of inertia, etc. Selection rules are discussed.

I. INTRODUCTION

IN Part I of this paper[1] the complete classical vibration problem of the tetrahedral X_2YZ_2 molecular model has been presented, including derivation of the normal coordinates, cubic and quartic parts of the anharmonic potential function, and components of vibrational angular momentum as well as discussion of the valence-type potential function. In Part II the quantum-mechanical calculation of the rotation-vibration energies of the X_2YZ_2 model is carried out to second-order approximation. The quantum-mechanical Hamiltonian is set up according to the method of Wilson and Howard[2] and, after contact transformation of the Hamiltonian according to the method discussed by Thomas,[3] Nielsen,[4] and Shaffer,[5] a perturbation calculation of the allowed energies is made.

II. CLASSICAL ROTATIONAL HAMILTONIAN

The kinetic energy of rotation of the nonvibrating model has the form

$$T_R=(1/2)\{I_{ex}\omega_x^2+I_{ey}\omega_y^2+I_{ez}\omega_z^2\}, \quad (1)$$

where the coordinate system xyz is the body-fixed system of principal axes defined in Section II of Part I and in terms of which the equilibrium products of inertia vanish; ω_x, ω_y, and ω_z are the components of the instantaneous angular velocity; the equilibrium values of the moments of inertia are

$$\begin{aligned} I_{ex}&=2mb_0^2+2n(do^2+e_0^2)+Mc_0^2,\\ I_{ey}&=2m(a_0^2+b_0^2)+2ne_0^2+Mc_0^2, \quad (2)\\ I_{ez}&=2ma_0^2+2nd_0^2, \end{aligned}$$

[1] W. H. Shaffer and R. C. Herman, J. Chem. Phys. **12**, 494 (1944).
[2] E. B. Wilson, Jr., and J. B. Howard, J. Chem. Phys. **4**, 262 (1936).
[3] L. H. Thomas, J. Chem. Phys. **10**, 532, 538 (1942).
[4] H. H. Nielsen, Phys. Rev. **60**, 794 (1941).
[5] Shaffer, Thomas, and Nielsen, Phys. Rev. **56**, 895, 1051 (1939).

where the masses and geometrical dimensions are the ones defined in Table I of Part I. The energy expression (1) can be expressed in Hamiltonian form as:

$$H_R=(1/2)\{P_x^2/I_{ex})+(P_y^2/I_{ey})+(P_z^2/I_{ez})\}, \quad (3)$$

where P_x, P_y, and P_z are the components of the total angular momentum of rotation of the model.

When the model vibrates, the moments of inertia have instantaneous values which depend on the normal coordinates, the instantaneous products of inertia are not zero but are functions of the normal coordinates and there is set up an internal angular momentum of vibration with components p_x, p_y, and p_z defined in Eqs. (16) of Part I. For the vibrating rotating model the rotational Hamiltonian becomes:

$$\begin{aligned}H_R=(1/2)\{&\mu_{xx}(P_x-p_x)^2+\mu_{yy}(P_y-P_y)^2\\&+\mu_{zz}(P_z-p_z)^2+2\mu_{xy}(P_x-p_x)(P_y-P_y)\\&+2\mu_{yz}(P_y-p_y)(P_z-p_z)\\&+2\mu_{zx}(P_z-p_z)(P_x-p_x)\}, \quad (4)\end{aligned}$$

where P_x, P_y, and P_z are the components of total angular momentum and the coefficients of inertia μ_{xx}, etc., can be expressed to second-order approximation in terms of the dimensionless normal coordinates defined in Eq. (12) of Part I:

$$\begin{aligned}
\mu_{xx}&=I_{ex}^{-1}\{1+\sum_i \omega_i^{-\frac{1}{2}}a_iq_i+\sum_h \omega_h^{-1}(a_h^2-a_{hh}+d_h^2+f_h^2)q_h^2+\cdots\},\\
\mu_{yy}&=I_{ey}^{-1}\{1+\sum_i \omega_i^{-\frac{1}{2}}b_iq_i+\sum_h \omega_h^{-1}(b_h^2-b_{hh}+d_h^2+e_h^2)q_h^2+\cdots\},\\
\mu_{zz}&=I_{ez}^{-1}\{1+\sum_i \omega_i^{-\frac{1}{2}}c_iq_i+\sum_h \omega_h^{-1}(c_h^2-c_{hh}+e_h^2+f_h^2)q_h^2+\cdots\},\\
\mu_{xy}&=(I_{ex}I_{ey})^{-\frac{1}{2}}\{\sum_j \omega_j^{-\frac{1}{2}}d_jq_j+\sum_h \omega_h^{-1}(e_hf_h-a_hd_h-b_hd_h)q_h^2+\cdots\},\\
\mu_{yz}&=(I_{ey}I_{ez})^{-\frac{1}{2}}\{\sum_l \omega_l^{-\frac{1}{2}}e_lq_l+\sum_h \omega_h^{-1}(d_hf_h-b_he_h-c_he_h)q_h^2+\cdots\},\\
\mu_{zx}&=(I_{ez}I_{ex})^{-\frac{1}{2}}\{\sum_k \omega_k^{-\frac{1}{2}}f_kq_k+\sum_h \omega_h^{-1}(d_he_h-a_hf_h-c_hf_h)q_h^2+\cdots\}.
\end{aligned} \quad (5)$$

The notation adopted in Part I will be used here, namely, the subscript h denotes any one of the nine normal coordinates; i assumes the values 1, 2, 3, 4, and denotes a coordinate of symmetry type A_1; j assumes the value 5 and denotes the coordinate of type A_2; k assumes values 6, 7, and denotes coordinates of type B_1; and l assumes values 8, 9, and denotes coordinates of type B_2. The coefficients a_i, a_{ii}, etc., occurring in Eqs. (5) are defined in the following equations in which $\tau=(\hbar/2\pi c)$; the quantities n_{sh} are coefficients in Eqs. (7), (8), (9), and (10) of Part I giving the relations between the intermediate and normal coordinates; the quantities $\xi_{hh'}$, $\eta_{hh'}$, and $\zeta_{hh'}$ are the Coriolis parameters defined in Eqs. (17) of Part I; and the equilibrium rotational constants are $B_{ex}=h/8\pi^2cI_{ex}$, $B_{ey}=h/8\pi^2cI_{ey}$, and $B_{ez}=h/8\pi^2cI_{ez}$:

$$\begin{aligned}
a_i&=8\tau^{-\frac{1}{2}}B_{ex}[m(b_0-c_0)n_{1i}-n(e_0+c_0)n_{2i}-nd_0n_{4i}],\\
b_i&=8\tau^{-\frac{1}{2}}B_{ey}[m(b_0-c_0)n_{1i}-n(e_0+c_0)n_{2i}+ma_0n_{3i}],\\
c_i&=8\tau^{-\frac{1}{2}}B_{ez}[ma_0n_{3i}-nd_0n_{4i}],
\end{aligned} \quad (6a)$$

$$a_j=b_j=c_j=0; \quad a_k=b_k=c_k=0; \quad a_l=b_l=c_l=0;$$

$$\begin{aligned}
a_{ii}&=2B_{ex}[\mu_1n_{1i}^2+\mu_2n_{2i}^2+\mu_4n_{4i}^2+2\mu_{12}n_{1i}n_{2i}-\xi_{8i}^2-\xi_{9i}^2],\\
b_{ii}&=2B_{ey}[\mu_1n_{1i}^2+\mu_2n_{2i}^2+\mu_3n_{3i}^2+2\mu_{12}n_{1i}n_{2i}-\eta_{6i}^2-\eta_{7i}^2],\\
c_{ii}&=2B_{ez}[\mu_3n_{3i}^2+\mu_4n_{4i}^2-\zeta_{5i}^2],
\end{aligned} \quad (6b)$$

$$\begin{aligned}
a_{55}&=2B_{ex}[2n(nd_0^2/ma_0^2)n_{55}^2-\xi_{65}^2-\xi_{75}^2],\\
b_{55}&=2B_{ey}[2nn_{55}^2-\eta_{85}^2-\eta_{95}^2],\\
c_{55}&=2B_{ez}[\mu_5n_{55}^2-\zeta_{51}^2-\zeta_{52}^2-\zeta_{53}^2-\zeta_{54}^2],
\end{aligned} \quad (6c)$$

$$
\begin{aligned}
a_{kk}&=2B_{ex}[(\mu_6-\mu_1)n_{6k}^2+(\mu_7-\mu_2)n_{7k}^2+2(\mu_{67}-\mu_{12})n_{6k}n_{7k}-\xi_{k5}^2],\\
b_{kk}&=2B_{ey}[\mu_6 n_{6k}^2+\mu_7 n_{7k}^2+2\mu_{67}n_{6k}n_{7k}-\eta_{k1}^2-\eta_{k2}^2-\eta_{k3}^2-\eta_{k4}^2],\\
c_{kk}&=2B_{ez}[\mu_1 n_{6k}^2+\mu_2 n_{7k}^2+2\mu_{12}n_{6k}n_{7k}-\zeta_{k8}^2-\zeta_{k9}^2],
\end{aligned}
\tag{6d}
$$

$$
\begin{aligned}
a_{ll}&=2B_{ez}[\mu_8 n_{8l}^2+\mu_9 n_{9l}^2+2\mu_{89}n_{8l}n_{9l}-\xi_{l1}^2-\xi_{l2}^2-\xi_{l3}^2-\xi_{l4}^2],\\
b_{ll}&=2B_{ey}[(\mu_8-\mu_1)n_{8l}^2+(\mu_9-\mu_2)n_{9l}^2+2(\mu_{89}-\mu_{12})n_{8l}n_{9l}-n_{l5}^2],\\
c_{ll}&=2B_{ex}[\mu_1 n_{8l}^2+\mu_2 n_{9l}^2+2\mu_{12}n_{8l}n_{9l}-\zeta_{l6}^2-\zeta_{l7}^2],
\end{aligned}
\tag{6e}
$$

$$
\begin{aligned}
&d_i=e_i=f_i=0,\\
&d_5=8B_{ex}^{\frac{1}{2}}B_{ey}^{\frac{1}{2}}(-nd_0n_{55}),\quad e_5=f_5=0,\quad d_k=e_k=0,\quad d_l=f_l=0,\\
&f_k=4B_{ex}^{\frac{1}{2}}B_{ey}^{\frac{1}{2}}[\{m(b_0-2c_0)+nb_0\}n_{6k}-2n(e_0+c_0)n_{7k}],\\
&e_l=8B_{ey}^{\frac{1}{2}}B_{ex}^{\frac{1}{2}}[m(b_0-c_0)n_{8l}-n(e_0+c_0)n_{9l}].
\end{aligned}
\tag{6f}
$$

The cross-product terms in Eqs. (5) and the corresponding coefficients in Eqs. (6) have been omitted for the sake of brevity since they do not ordinarily contribute to the energies up to second-order approximation.

III. THE QUANTUM-MECHANICAL HAMILTONIAN

The appropriate quantum-mechanical Hamiltonian operator for the rotating vibrating tetrahedral X_2YZ_2 molecular model can be set up according to the method of Wilson and Howard in the form

$$
H=(1/2)\sum_{\alpha}\sum_{\beta}\mu_{\alpha\beta}(P_\alpha-p_\alpha)(P_\beta-p_\beta)+(hc/2\hbar^2)\sum_{h}\omega_h(\mu^{\frac{1}{2}}p_h\mu^{-\frac{1}{2}}p_h)+U, \tag{7}
$$

where α and β denote the axes x, y, and z; $\mu_{\alpha\beta}$ denotes one of the inertia coefficients defined in Eqs. (5); μ is the determinant of the $\mu_{\alpha\beta}$; p_h is the operator corresponding to the dimensionless normal coordinate q_h; P_α is the operator corresponding to the component of total angular momentum; $p_\alpha=\sum_h X_{\alpha h}p_h$ is the operator corresponding to the α-component of vibrational angular momentum if $X_{\alpha h}$ is one of the quantities defined in Eqs. (17) of Part I; U is the potential energy function. The zero-, first-, and second-order parts of the Hamiltonian operator are

$$
H_0=(hc/2)\{\sum_{h=1}^{9}\omega_h[(p_h^2/\hbar^2)+q_h^2]+(2/\hbar^2)[B_{ex}P_x^2+B_{ey}P_y^2+B_{ez}P_z^2]\}, \tag{8a}
$$

$$
\begin{aligned}
H_1=U_1+(hc/\hbar^2)\{&\sum_{i=1}^{4}\omega_i^{-\frac{1}{2}}q_i[a_iB_{ex}P_x^2+b_iB_{ey}P_y^2+c_iB_{ez}P_z^2]+\omega_5^{-\frac{1}{2}}q_5d_5B_{ex}^{\frac{1}{2}}B_{ey}^{\frac{1}{2}}(P_xP_y+P_yP_x)\\
&+\sum_{l=8}^{9}\omega_l^{-\frac{1}{2}}q_le_lB_{ey}^{\frac{1}{2}}B_{ez}^{\frac{1}{2}}(P_yP_z+P_zP_y)+\sum_{k=6}^{7}\omega_k^{-\frac{1}{2}}q_kf_kB_{ez}^{\frac{1}{2}}B_{ex}^{\frac{1}{2}}(P_zP_x+P_xP_z)\\
&-2(B_{ex}p_xP_x+B_{ey}p_yP_y+B_{ez}p_zP_z)\},
\end{aligned}
\tag{8b}
$$

$$
\begin{aligned}
H_2=U_2+(hc/\hbar^2)\{&\sum_{h=1}^{9}\omega_h^{-1}q_h^2[(a_h^2-a_{hh}+d_h^2+f_h^2)B_{ex}P_x^2+(b_h^2-b_{hh}+e_h^2+d_h^2)B_{ey}P_y^2\\
&+(c_h^2-c_{hh}+e_h^2+f_h^2)B_{ez}P_z^2]+(B_{ex}p_x^2+B_{ey}p_y^2+B_{ez}p_z^2)\}.
\end{aligned}
\tag{8c}
$$

The straightforward determination of the eigenvalues of $H=H_0+H_1+H_2$ by means of a perturbation calculation is complicated because of the large number of variables involved and the fact that the tetrahedral X_2YZ_2 model is an asymmetric rotator. The perturbation calculation is simplified by a contact transformation of the Hamiltonian of the type THT^{-1} described by Thomas,[3] Nielsen,[4] and Shaffer;[5] it is possible to transform from H_1 into H_2 all those terms which contribute only to the second-order energy E_2. If the general matrix element of the transformed Hamiltonian diagonal in all the vibrational quantum numbers is computed with the angular coordinates and total angular

momentum operators treated as constants, the result yields (1) the purely vibrational contribution E_v to the eigenvalues of H and (2) a modified rotational Hamiltonian H_R in which the rotational constants B_{ex}, etc. are replaced by B_{vx}, etc., effective in the respective vibrational states. The eigenvalues of H_R must be found from a secular determinant.

IV. THE VIBRATIONAL TERM

The purely vibrational contribution E_v to the eigenvalues of the vibration-rotation Hamiltonian can be written in the form, $E_v=hcG$, where G is the vibrational term and is expressed in cm^{-1}. A detailed calculation shows that G can be expressed in the form

$$G=G_0+\sum_{h=1}^{9}\omega_h(v_h+\tfrac{1}{2})+\sum_h[G_{hh}(v_h+\tfrac{1}{2})^2+\sum_{h'<h}G_{hh'}(v_h+\tfrac{1}{2})(v_{h'}+\tfrac{1}{2})], \tag{9}$$

where v_h denotes the vibrational quantum number which is associated with the hth normal frequency ω_h and may assume positive integral values; G_0 is a small constant term which occurs in the second-order energy correction and the quantities G_{hh} and $G_{hh'}$ are the functions of the anharmonic constants, Coriolis parameters, etc., defined below in Eqs. (11).

It is convenient in the definition of the G_{hh} to introduce the following abbreviations:

$$\begin{aligned}
D_{hh'h''}&=[(\omega_h+\omega_{h'}+\omega_{h''})(\omega_h-\omega_{h'}-\omega_{h''})(\omega_h-\omega_{h'}+\omega_{h''})(\omega_h+\omega_{h'}-\omega_{h''})]^{-1},\\
E_{hh'}&=[(8\omega_h^2-3\omega_{h'}^2)/(4\omega_h^2-\omega_{h'}^2)],\\
F_{hh'}&=[2\omega_h/(4\omega_h^2-\omega_{h'}^2)],\\
C_{hh'h''}&=[\omega_h^2(\omega_h^2-\omega_h^2-\omega_{h''}^2)D_{hh'h''}/2],\\
K_{hh'}&=[(\omega_h/\omega_{h'})+(\omega_{h'}/\omega_h)],\\
H_{hh'}&=[\omega_{h'}/(4\omega_h^2-\omega_{h'}^2)].
\end{aligned} \tag{10}$$

The quantities G_0, G_{hh}, and $G_{hh'}$ are given by the following relations, in which the system of subscript notation is that which was described in Section II:

$$\begin{aligned}
G_0=&(1/4)\sum_h\{(a_{hh}+b_{hh}+c_{hh})-(3/8)(a_i^2+b_i^2+c_i^2)+(1/4)(a_ib_i+b_ic_i+c_ia_i)-(d_j^2+e_l^2+f_k^2)\\
&+(3/2)\gamma_{hhhh}\}-(1/16)\sum_h\{7\omega_i^{-1}\beta_{iii}^2+4\omega_i\omega_{i'}\omega_{i''}D_{ii'i''}\beta_{ii'i''}^2+4\omega_i\omega_k\omega_{k'}D_{ikk'}\beta_{ikk'}^2\\
&+4\omega_i\omega_l\omega_{l'}D_{ill'}\beta_{ill'}^2+4\omega_j\omega_k\omega_l\beta_{jkl}^2-3H_{ii'}\beta_{iii'}^2-3H_{ji}\beta_{jji}^2-3H_{ki}\beta_{kki}^2-3H_{li}\beta_{lli}^2\}\\
&-(1/2)\sum_{h,h'}\{(\xi_{kj}^2+\xi_{li}^2)B_{ex}+(\eta_{ij}^2+\eta_{ki}^2)B_{ey}+(\zeta_{ij}^2+\zeta_{kl}^2)B_{ez}\},\\
G_{ii}=&(1/4)\{6\gamma_{iiii}-15\omega_i^{-1}\beta_{iii}^2-\sum_{i'}\omega_{i'}^{-1}E_{ii'}\beta_{iii'}^2\},\\
G_{jj}=&(1/4)\{6\gamma_{jjjj}-\sum_i\omega_i^{-1}E_{ji}\beta_{jji}^2\},\\
G_{kk}=&(1/4)\{6\gamma_{kkkk}-\sum_i\omega_i^{-1}E_{ki}\beta_{kki}^2\},\\
G_{ll}=&(1/4)\{6\gamma_{llll}-\sum_i\omega_i^{-1}E_{li}\beta_{lli}^2\},\\
G_{ii'}=&\{\gamma_{iii'i'}-3\omega_i^{-1}\beta_{iii}\beta_{ii'i'}-3\omega_{i'}^{-1}\beta_{i'i'i'}\beta_{i'ii}-\sum_{i''}(\omega_{i''}^{-1}\beta_{iii''}\beta_{i'i'i''})\\
&-F_{ii'}\beta_{iii'}^2-F_{i'i}\beta_{i'i'i}^2-\sum C_{i''ii'}\beta_{ii'i''}^2\},\\
G_{ij}=&\{\gamma_{iijj}-3\omega_i^{-1}\beta_{iii}\beta_{jji}-F_{ji}\beta_{jji}^2+K_{ij}\zeta_{ij}^2B_{ez}\},\\
G_{ik}=&\{\gamma_{iikk}-3\omega_i^{-1}\beta_{iii}\beta_{kki}-F_{ki}\beta_{kki}^2+K_{ki}\eta_{ki}^2B_{ey}-\sum_{k'}C_{k'ki}\beta_{ikk'}^2\},
\end{aligned} \tag{11}$$

$$G_{il}=\{\gamma_{iill}-3\omega_i^{-1}\beta_{iii}\beta_{lli}-F_{li}\beta_{lli}^2+K_{li}\xi_{li}^2B_{ez}-\sum_{l'}C_{l'li}\beta_{ill'}^2\},$$

$$G_{jk}=\{\gamma_{jjkk}+K_{jk}\xi_{jk}^2B_{ez}-\sum_{l}C_{ljk}\beta_{jkl}^2\},$$

$$G_{jl}=\{\gamma_{jjll}+K_{jl}\eta_{jl}^2B_{ey}-\sum_{k}C_{klj}\beta_{jkl}^2\},$$

$$G_{kl}=\{\gamma_{kkll}+K_{kl}\zeta_{kl}^2B_{ez}-\sum_{j}C_{jkl}\beta_{jkl}^2\},$$

$$G_{kk'}=\{\gamma_{kkk'k'}-\sum_{i}C_{ikk'}\beta_{ikk'}^2\},$$

$$G_{ll'}=\{\gamma_{ill'l'}-\sum_{i}C_{ill'}\beta_{ill'}^2\}.$$

V. THE ROTATIONAL TERM F

The effective rotational Hamiltonian H_R, which results from the contact transformation and subsequent diagonalization with respect to the vibrational coordinates, has the form:

$$H_R=(hc/\hbar^2)\{B_{vx}P_x^2+B_{vy}P_y^2+B_{vz}P_z\}-H_{RC}, \tag{12}$$

in which H_{RC} contains the terms associated with centrifugal stretching of the molecule and has the form:

$$H_{RC}=(hc/\hbar^4)\{\tau_1P_x^4+\tau_2P_y^4+\tau_3P_z^4+\tau_4(P_xP_y+P_yP_x)^2+\tau_5(P_yP_z+P_zP_y)^2+\tau_6(P_zP_y+P_xP_z)^2$$
$$+\tau_7(P_x^2P_y^2+P_y^2P_x^2)+\tau_8(P_x^2P_z^2+P_z^2P_x^2)+\tau_9(P_y^2P_z^2+P_z^2P_y^2)\}, \tag{13}$$

where

$$\tau_1=B_{ex}^2\sum_i(a_i^2/2\omega_i^2);\quad \tau_2=B_{ey}^2\sum_i(b_i^2/2\omega_i^2);\quad \tau_3=B_{ez}^2\sum_i(c_i^2/2\omega_i^2);$$

$$\tau_4=B_{ex}B_{ey}\sum_j(d_j^2/2\omega_j^2);\quad \tau_5=B_{ey}B_{ez}\sum_l(e_l^2/2\omega_l^2);\quad \tau_6=B_{ex}B_{ez}\sum_k(f_k^2/2\omega_k^2);$$

$$\tau_7=B_{ex}B_{ey}\sum_i(a_ib_i/2\omega_i^2);\quad \tau_8=B_{ex}B_{ez}\sum_i(a_ic_i/2\omega_i^2);\quad \tau_9=B_{ey}B_{ez}\sum_i(b_ic_i/2\omega_i^2).$$

The effective rotational constants are, to second-order approximation,

$$B_{vx}=B_{ex}\{1+\sum_{h=1}^{9}\alpha_h(v_h+\tfrac{1}{2})\},\quad B_{vy}=B_{ey}\{1+\sum_{h=1}^{9}\beta_h(v_h+\tfrac{1}{2})\},\quad B_{vz}=B_{ez}\{1+\sum_{h=1}^{9}\gamma_h(v_h+\tfrac{1}{2})\}, \tag{14}$$

where if $J_{hh'}=[(3\omega_h^2+\omega_{h'}^2)/(\omega_h^2-\omega_{h'}^2)]$ and $A=[3\beta_{iii}+\beta_{ii'i'}+\beta_{ijj}+\beta_{ikk}+\beta_{ill}]$,

$$\alpha_i=\omega_i^{-1}\{a_i^2-a_{ii}+\omega_i^{-1}a_iA+2B_{ex}\sum_l J_{il}\xi_{li}^2\},$$

$$\beta_i=\omega_i^{-1}\{b_i^2-b_{ii}+\omega_i^{-1}b_iA+2B_{ey}\sum_k J_{ik}\eta_{ki}^2\}, \tag{15a}$$

$$\gamma_i=\omega_i^{-1}\{c_i^2-c_{ii}+\omega_i^{-1}c_iA+2B_{ez}\sum_j J_{ij}\zeta_{ji}^2\},$$

$$\alpha_j=\omega_j^{-1}\{d_j^2-a_{jj}+2B_{ex}\sum_k J_{jk}\xi_{kj}^2\},$$

$$\beta_j=\omega_j^{-1}\{d_j^2-b_{jj}+2B_{ey}\sum_l J_{jl}\eta_{jl}^2\}, \tag{15b}$$

$$\gamma_j=\omega_j^{-1}\{-c_{jj}+2B_{ez}\sum_i J_{ji}\zeta_{ji}^2\},$$

$$\alpha_k=\omega_k^{-1}\{f_k^2-a_{kk}+2B_{ez}\sum_j J_{kj}\xi_{kj}^2\},$$

$$\beta_k=\omega_k^{-1}\{-b_{kk}+2B_{ey}\sum_i J_{ki}^2\eta_{ki}^2\},\tag{15c}$$
$$\gamma_k=\omega_k^{-1}\{f_k^2-c_{kk}+2B_{ez}\sum_l J_{kl}^2\zeta_{kl}^2\},$$
$$\alpha_l=\omega_l^{-1}\{-a_{ll}+2B_{ex}\sum_i J_{li}^2\xi_{li}^2\},$$
$$\beta_l=\omega_l^{-1}\{e_l^2-b_{ll}+2B_{ey}\sum_j J_{lj}^2\eta_{lj}^2\},\tag{15d}$$
$$\gamma_l=\omega_l^{-1}\{e_l^2-c_{ll}+2B_{ez}\sum_k J_{lk}^2\zeta_{lk}^2\}.$$

The eigenvalues of H_R can be evaluated from a secular determinant which is a modified form of the one given by Wang[6] for the rigid asymmetric rotator. The determinant can conveniently be set up in terms of the usual rotator quantum numbers, J for total angular momentum, K for the z component, and M for the space-fixed Z component where J may assume the values 0, 1, 2, $\cdots$; K assumes the values 0, ±1, ±2, $\cdots$, $\pm J$; and M assumes the values 0, ±1, ±2, $\cdots$, $\pm J$. The secular determinant breaks up into $(2J+1)$-fold steps in each of which J and M are constant and K assumes its $(2J+1)$ possible values. The non-vanishing elements of each step are of three general types, which have the following forms if $f=J(J+1)$:

$$\begin{aligned}
&(JKM|H_R|JKM)=hc\{R_1+R_2K^2+R_3K^4\},\\
&(JKM|H_R|JK\pm2M)=hc\{R_4+R_5[(K\pm2)^2+K^2]\}\{f-K(K\pm1)\}^{\frac{1}{2}}\{f-(K\pm1)(K\pm2)\}^{\frac{1}{2}},\\
&(JKM|H_R|JK\pm4M)=hcR_6\{f-K(K\pm1)\}^{\frac{1}{2}}\{f-(K\pm1)(K\pm2)\}^{\frac{1}{2}}\{f-(K\pm2)(K\pm3)\}^{\frac{1}{2}}\\
&\qquad\qquad\times\{f-(K\pm3)(K\pm4)\}^{\frac{1}{2}},
\end{aligned}\tag{16}$$

where

$$\begin{aligned}
R_1&=(f/4)[2(B_{vx}+B_{vy})+\tau_1+\tau_2+4\tau_4-2(\tau_5+\tau_6+\tau_7)]+(f^2/8)[-3\tau_1-3\tau_2-4\tau_4-2\tau_7],\\
R_2&=(1/8)[8B_{vz}-4(B_{vx}+B_{vy})-5\tau_1-5\tau_2-20(\tau_4-\tau_5-\tau_6)+10\tau_7]\\
&\qquad+(f/4)[3\tau_1+3\tau_2+4\tau_4-8\tau_5-8\tau_6+2\tau_7-4\tau_8-4\tau_9],\\
R_3&=(1/8)[-3\tau_1-3\tau_2+8\tau_3-12\tau_4+16(\tau_5+\tau_6)-2\tau_7+8(\tau_8+\tau_9)],\\
R_4&=(1/4)[(B_{vx}-B_{vy})+5(\tau_6-\tau_5)-f(\tau_1-\tau_2)],\\
R_5&=(1/8)[\tau_1-\tau_2-4\tau_6+4\tau_5-2\tau_8+2\tau_9],\\
R_6&=(1/16)[-\tau_1-\tau_2+4\tau_4+2\tau_7].
\end{aligned}$$

The eigenvalues of H_R obtained from the secular determinant can be expressed in the form $E_R=hcF$, where F is the rotational term. A method has been discussed by Shaffer and Nielsen[7] and Nielsen[8] whereby it is possible to factor each JM step of the secular determinant into four steps and thereby facilitate the evaluation of the rotational term, F.

VI. SELECTION RULES

The vibrational selection rules were stated in Section II of Part I. The rotational selection rules are those given by Dennison[9] for the asymmetric rotator. Dennison has also discussed the effect of the identical particles on intensities of the rotational lines in the rotation-vibration bands.

[6] S. C. Wang, Phys. Rev. **34**, 243 (1929).
[7] W. H. Shaffer and H. H. Nielsen, Phys. Rev. **56**, 188 (1939).
[8] H. H. Nielsen, Phys. Rev. **59**, 565 (1941).
[9] D. M. Dennison, Rev. Mod. Phys. **3**, 280 (1931).

Further Studies of the Structure and Stability of Burner Flames[1-3]

GUENTHER VON ELBE AND MORRIS MENTSER
Central Experiment Station, Bureau of Mines, Pittsburgh, Pennsylvania

(Received September 23, 1944)

It is shown that, contrary to Mache's model of the progressive extinction of a flame from the burner rim, a combustion zone cannot vanish within a combustible stream. The depth of penetration of the quenching of the explosive reaction by the burner wall is calculated from values of burning velocity and critical boundary velocity gradient for flashback; it is compared with the limiting distance between plane-parallel plates and the limiting tube diameter for flame propagation. The thermal expansion of the gas normal and parallel to the combustion zone is discussed. An experimental analysis and discussion of partial entrance of the combustion zone into the burner tube (tilted flame) and partial attachment to the burner rim are given. New data have been obtained on hydrogen and acetylene flames. For instantaneous flashback, the boundary velocity gradients are independent of tube diameter, as expected; these gradients are not a satisfactory criterion for flame stability because flashback can be readily induced by tilted flames. The limit of the tilted-flame range is represented by the semitheoretical equation

$$g/(1-4S_u/gR)^{\frac{1}{2}}=\text{const.}$$

g is the boundary-velocity gradient, S_u the burning velocity, and R the tube diameter. The boundary-velocity gradients for blow-off are again found constant over the laminar flow range. The compression of acetylene-oxygen streams by the combustion zone has been measured. The burning velocities calculated from these and additional thermodynamic data agree well with those determined from gas flow and cone surface.

IN a previous paper,[4] the flashback and blow-off of burner flames, the pattern of the gas flow, and the distribution of gas velocity and temperature have been investigated theoretically and experimentally. The experiments were made with mixtures of natural gas and air. The present paper contains additional observations on flames of mixtures of hydrogen and acetylene with air and oxygen, and a discussion of several points that have not been fully treated before.

In this, as in the previous paper, the term "combustion zone" is synonymous to the frequently used terms "explosion wave" or "flame front." It denotes the narrow preheating and reaction zone which separates the burned from the unburned gas. Within the zone, in the layers adjacent to the completely burned gas, heat is released and atoms and free radicals are formed by the chemical reaction; a part of the heat and active species (chain carriers) is transferred by conduction and diffusion to the adjoining layers of unburned gas which in turn become activated to rapid chemical reaction. In this way, the combustion zone progresses against the unburned gas at a definite velocity S_u, the burning velocity, whose magnitude is evidently affected by any factors which modify the reaction rate and the rates of heat transfer and diffusion into the unburned gas. Thus, at a certain distance from a solid wall, the burning velocity decreases to zero, and this distance becomes smaller as the temperature of the wall is raised.

The combustion zone is generally plainly visible owing to chemiluminescence, notably by emission of CC and CH bands; and if the zone retains a fixed position against a gas stream issuing from a burner port, it forms the well-known inner flame cone.

I. SUPPLEMENTAL DISCUSSION OF THE STABILITY AND STRUCTURE OF BURNER FLAMES

(A) The Propagation and Structure of the Combustion Zone

While the work of Mache[5] has materially contributed to the theory of burner flames, it appears

[1] Published by permission of the Director, Bureau of Mines, U. S. Department of the Interior.

[2] From a thesis submitted by Morris Mentser to the faculty of the Graduate School of the University of Pittsburgh in partial fulfillment of the requirements for the degree of Master of Science.

[3] Contribution from the Central Experiment Station, Bureau of Mines, U. S. Department of the Interior.

[4] B. Lewis and G. von Elbe, J. Chem. Phys. **11**, 75 (1943).

[5] H. Mache, *Die Physik der Verbrennungserscheinungen* (Veit und Comp., Leipzig, 1918), pp. 25–54.

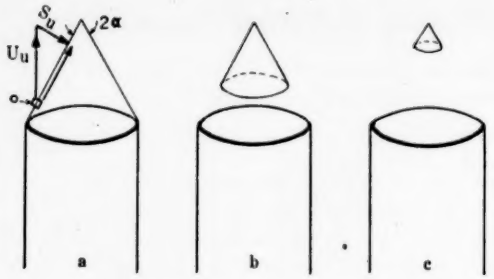

FIG. 1. Illustration of Mache's concept of progressive extinction of the combustion zone from the rim of the burner port.

that neither this author nor subsequent investigators have taken sufficient account of the mechanism of propagation of the combustion zone. Thus, an erroneous concept has persisted in the literature regarding a supposed tendency of the burner flame to extinguish itself progressively from the rim toward the stream axis. This is illustrated in Fig. 1. For simplicity, the gas velocity U_u is taken as uniform over the cross section of the stream issuing from the burner port. An inner cone is supposed to have been formed with an opening angle 2α so that $S_u = U_u \sin\alpha$; that is, the burning velocity is everywhere equal to the normal component of the gas velocity, and a necessary condition for the stability of the cone is thus fulfilled. It is now further argued that any element of the combustion zone (as, for example, the element at point O) is simultaneously carried upward by the gas flow with the velocity U_u and inward by the combustion with the velocity S_u and that consequently the element moves along the resultant of the vectors U_u and S_u within the cone surface at a velocity $U_u \cos\alpha$. On this basis it would appear, as illustrated according to Mache in Figs. 1b and 1c, that an element at the rim moves within the combustion zone toward the cone tip; that is, the cone is progressively extinguished from the rim toward the tip. To maintain a stationary cone, Mache assumes that the combustion zone is continually restored at the cone base by a virtual pilot flame which is maintained by a supposed slow-moving, turbulent boundary layer surrounding the gas stream.

To visualize the consequences of this concept, consider an elementary tube extending normal to the combustion zone from the element O into the unburned gas. This tube encloses all the gas elements that enter the combustion zone successively at points above O, and the tube moves correspondingly upward. Since, in the absence of a pilot flame at the cone base, the gas at lower points is supposed to remain unignited, it is virtually assumed that the reaction-inducing flow of heat and chain-carriers from the successively burning gas elements propagates only within the tube. This is certainly not the case. Rather, the progress of a combustion zone may be visualized in accordance with the principles of Huygen's construction for the propagation of a wave front, as shown schematically in Fig. 2A. A gas element entering the combustion zone is activated to rapid chemical reaction by contributions of heat and chain-carriers, not only from the preceding gas element in the same stream tube, but also from gas elements in the adjoining stream tubes; in turn it activates, not only the succeeding gas element in its own stream tube, but also the elements in adjoining stream tubes. Thus, ignition spreads from any point of the combustion zone laterally as well as forward; accordingly, a combustion zone cannot vanish within a combustible stream as Fig. 1 would indicate; rather, it always tends to occupy the whole cross section of the stream and moves as a unit with or against the stream or remains stationary, as the case may be. The combustion zone moves with the stream—the flame blows off—when the gas velocity everywhere exceeds the burning velocity; it moves against the stream —the flame flashes back—when the burning

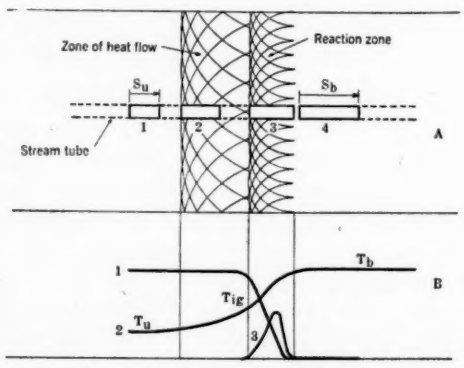

FIG. 2. A. Schematic view of the combustion zone. B. Temperature and concentration gradients within the combustion zone. 1. Concentration of fuel gas. 2. Temperature. 3. Concentration of atoms and free radicals.

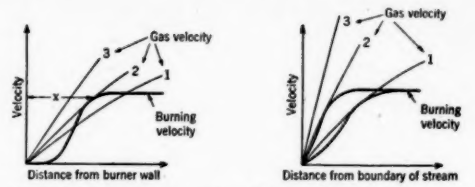

(a) Velocity gradients at wall of burner tube. Curve 1, flash-back; curve 2, flash-back limit; curve 3, no flash-back.

(b) Velocity gradients at boundary of stream above orifice. Curve 1, stable flame; curve 2, blow-off limit; curve 3, blow-off.

FIG. 3. Illustration of flashback and blow-off conditions.

velocity exceeds the gas velocity at any one point; and the flame remains stationary when the burning velocity equals the gas velocity at any one point but does not exceed it anywhere.

Other details of the combustion zone that are shown schematically in Fig. 2 are self-explanatory. In accordance with previous practice, the subscripts u and b refer to unburned and burned gas, respectively. The temperature at the beginning of the zone of active chemical reaction may be referred to as the ignition temperature T_{ig}; it obviously bears little relation to the ignition temperatures determined by heating or adiabatically compressing a combustible mixture to the point of explosion because the ignition process is controlled by other factors besides temperature.

(B) Depth of Penetration of the Quenching of the Explosive Reaction by the Burner Wall

It has been shown previously that a burner flame remains stable between two critical values of the gradient of gas velocity at the stream boundary.[4] For laminar flow in cylindrical tubes the gradient g may be written as a function of the total gas flow V and the radius R,

$$\lim_{r \to R} \left(\frac{-dU}{dr} \right) = g = 4V/\pi R^3. \qquad (1)$$

If subscripts F and B refer to the flashback and blow-off condition, respectively, then g_F and g_B are the lower and upper critical values of the velocity gradient between which the flame is stable. The conditions near the stream boundary are illustrated in Figs. 3a and 3b. The values of g_F and g_B obviously represent the slopes of the gas velocity curves 2 in the corresponding diagrams. With reference to Fig. 3a, the distance X from the wall over which the burning velocity is below its normal value may be defined as the depth of penetration of the quenching of the explosive reaction by the burner wall. It can be calculated approximately from measured values of g_F and S_u by assuming that, at the point of contact of the curves of burning velocity and critical gas velocity, the burning velocity is close to its normal measured value. It then follows that

$$X = S_u/g_F. \qquad (2)$$

The value X may be considered a measure for the limiting distance between plane parallel plates and, correspondingly, for the limiting diameter of cylindrical tubes below which flame propagation is quenched. The validity is only approximate, since X refers to a single wall bordering on a large volume of gas, whereas the quenching effects of two opposing walls merge and augment each other. Hence, the limiting

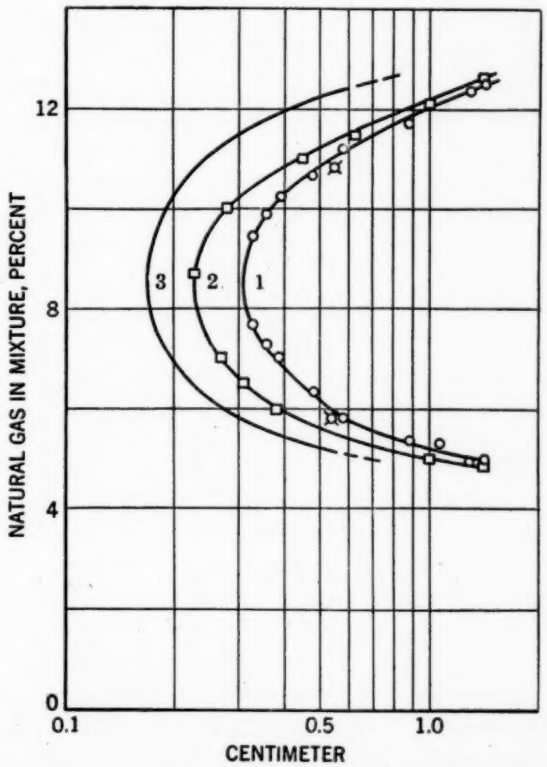

FIG. 4. Depth of penetration of the quenching of the explosive reaction by the burner wall. Natural gas-air mixtures. Curve 1, limiting diameter of cylindrical tubes for downward flame propagation (○ data by Lewis and von Elbe; ☼ new data). Curve 2, limiting distance between plane parallel plates for downward flame propagation. Curve 3, depth of penetration calculated from critical velocity gradients for flashback.

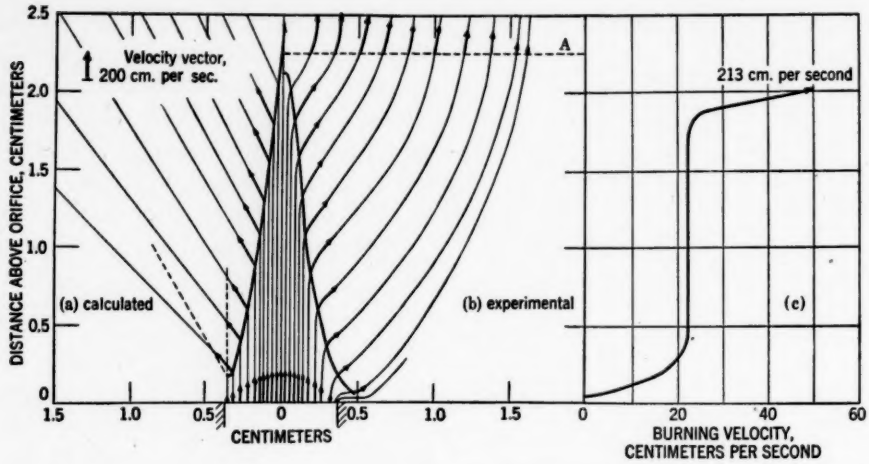

FIG. 5. Diagram of vertical center plane of natural gas-air flame on rectangular burner tube of 0.755×2.19 cm cross section. Mixture composition, 7.5 percent natural gas; flow, 204 cubic centimeters per second. (a) and (b): Combustion zone and flow pattern. (c) Burning velocity.

distance between plane parallel plates is larger than X and may, in the absence of a quantitative theory, be estimated to be comparable to $2X$. The limiting diameter of cylindrical tubes is even larger because of the additional effect of curvature. This is illustrated in Fig. 4. Curve 1 represents previously obtained data[4] with two new points added in order to insure that the composition of the natural gas had not changed appreciably in the interval between previous and present experiments. Curve 2 represents observations on a burner formed by two plane parallel plates, one fixed and the other movable. Curve 3 represents values of $2X$ calculated from previously published data of g_F and S_u.[4] It is seen that the limiting distance between plane parallel plates is even larger than $2X$, although not greatly so. The data of Fig. 4 refer to walls at room temperature; as the temperature is increased, the depth of penetration decreases.

It is of interest to report an observation by F. A. Smith[6] that a mixture of $2H_2+O_2$ flashed back in a cold glass tube of 0.013-inch (0.033-cm) diameter. For this mixture g_F is found to be 1.3×10^5 sec.$^{-1}$ (see Fig. 8) and S_u, according to Jahn,[7] is 870 cm per second. The value of X is, therefore, 0.0067 cm which accords well with Smith's observation.

[6] *Combustion* (American Gas Association, New York, 1932), 3rd edition, p. 110.
[7] G. Jahn, *Der Zündvorgang in Gasgemischen* (Oldenbourg, Berlin, 1934), p. 21.

(C) Modification of the Gas Flow at Tip and Base of the Conical Combustion Zone

In Fig. 5, a previous analysis[4] of a flame cone and flow pattern is reproduced with an additional curve showing the change of burning velocity over the cone surface. The analysis shows that the gas elements that enter the combustion zone in the range of constant burning velocity between tip and base expand only in the direction normal to the zone. At the tip and base, however, thermal expansion also takes place parallel to the combustion zone. In the axial stream tube, the expansion appears to be almost completely of the latter type, since the experimental records of this and other flames show that there is no appreciable change of gas velocity between unburned and burned gas in the central flow line. This lateral expansion at the cone tip is made possible by the divergence of the flow lines caused by refraction in the combustion zone. At the base the expanding gas elements acquire considerable velocity components parallel to the combustion zone in the direction of the free atmosphere. This is clearly shown by the outermost flow lines of Fig. 5b. Since the acceleration of the gas elements results in opposing inertia forces, the expansion parallel to the combustion zone in the inner flow lines is gradually checked, and thermal expansion normal to the zone predominates.

In the original photographs, the flow lines are

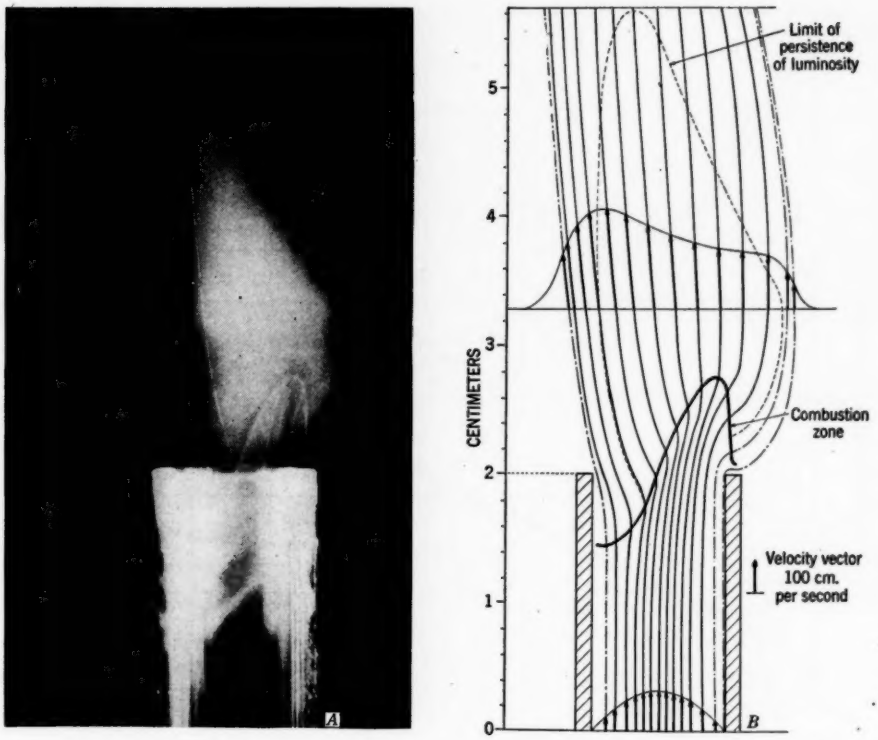

FIG. 6. Flame of natural gas and air, partially drawn into burner tube at gas flow just exceeding critical flow for flashback. Mixture composition, 8.1 percent natural gas in air; gas flow, 52 cc per second; inside diameter of tube, 1.068 cm. A. Photograph with particle tracks in vertical center plane (cf. Lewis and von Elbe, reference 4). B. Diagram of flow pattern and velocity distribution. Solidly-drawn flow lines are so located that the mass flow between any two adjoining lines is the same.

seen to diverge slightly even before entering the heating zone. It may be remembered that the combustion zone exerts a pressure on the unburned gas because of the acceleration of the gas flow.[5] This acceleration is smaller at the base of the cone than elsewhere because the burning velocity there is lower. Consequently, there exists a pressure drop in the unburned gas below the combustion zone from the stream center to the burner rim which appears to be the cause of the observed divergence of the flow lines.

(D) The Tilted Flame

A flame form, frequently observed when the gas flow is gradually reduced toward the flashback condition, is typified by the diagram in Fig. 6. It has already been described briefly.[4] The dynamic symmetry of the gas stream is destroyed: The combustion zone has partly entered the burner tube and exerts a pressure normal to the tube axis which causes a deflection of the stream of unburned gas in the opposite direction. The resulting change of velocity distribution in the unburned gas causes a decrease of the boundary velocity gradient, below the critical flashback value, in the region where the flame penetrates into the tube; this permits the combustion zone to propagate against the stream. As the combustion zone travels downward, the resistance of the flow of unburned gas to the deflecting pressure increases until a position of equilibrium is reached, in which the boundary velocity gradient at the deepest point of penetration has become equal to the critical gradient for flashback, but exceeds the critical value at lower points in the burner tube. Obviously, the equilibrium position is maintained only when the burner tube is cooled sufficiently. Generally, as the tube temperature increases, the combustion zone continues to travel downward, and flashback results.

When the gas flow is gradually increased

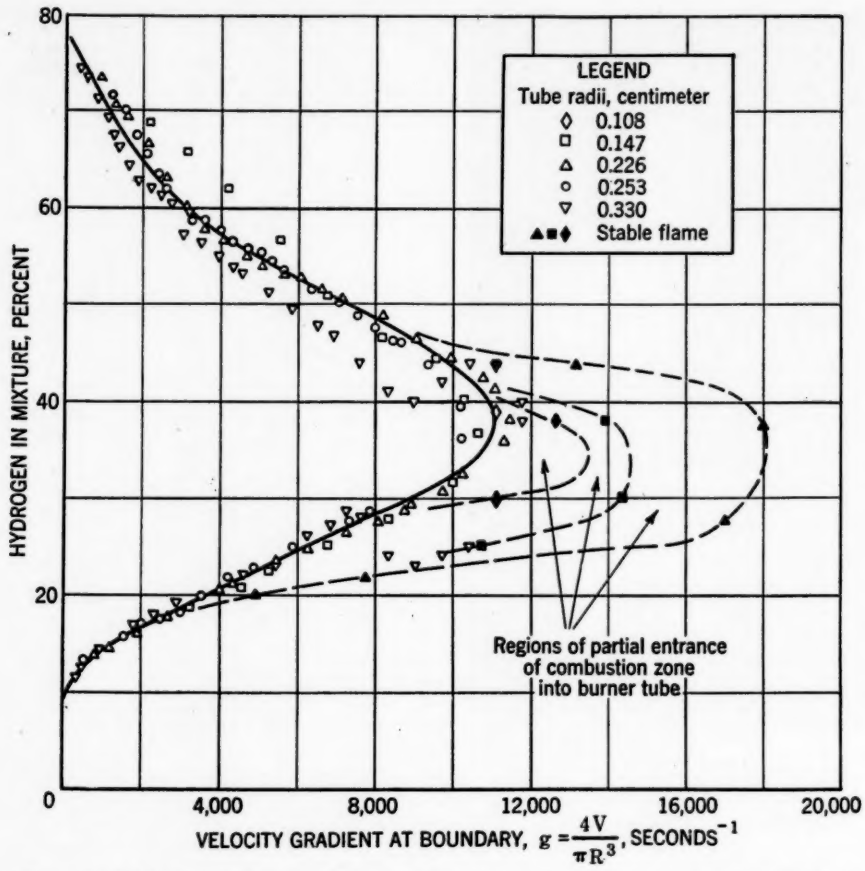

FIG. 7. Critical velocity gradients at boundary of gas stream for flashback of hydrogen-air flames in cylindrical water-cooled tubes of different diameters.

toward the blow-off condition, the combustion zone often remains attached to the port rim at a single point and extends from there at a steep angle over the gas stream. The phenomenon is analogous to the foregoing: The pressure exerted by the combustion zone deflects the flow lines in the unburned gas so that the boundary velocity gradient at the point of attachment is smaller than the critical gradient for blow-off. At all other points along the port rim, the critical gradient is exceeded. On further, usually slight, increase of the gas flow, the flame blows off completely.

Tilted flames, such as are shown in Fig. 6, are formed only below some critical flow which is a function of tube diameter. It is obviously desirable to determine this function theoretically, but the problem appears to be rather difficult and has not been completely solved. Nevertheless, it has been found possible to arrive at a semi-empirical equation with the aid of theoretical considerations. The equation is given in the following experimental part of the paper.

II. EXPERIMENTS ON HYDROGEN AND ACETYLENE FLAMES

(A) Apparatus and Procedure

The two gases, comprising the gas mixture to be studied, were passed individually through calibrated flowmeters into a mixing chamber. Effective mixing was accomplished by directing the two jets in the chamber at a right angle against each other (see, for example, Rummel[8]). On leaving the chamber, the gas mixture entered directly into a vertically mounted burner tube whose tip was surrounded by a water jacket. The gas was ignited by approaching the stream near the rim of the tube with a small flame.

[8] K. Rummel, *Der Einfluss des Mischvorganges auf die Verbrennung von Gas und Luft in Feuerungen* (Verlag Stahleisen, Düsseldorf, 1937).

For all experiments hydrogen, oxygen, and acetylene were supplied from tanks of compressed gas, while natural gas and air were taken from the lines in the laboratory. No purification of these gases was considered necessary, other than the removal of water vapor from the air by passing it through a calcium chloride trap.

Flowmeters for small rates of gas flow (rates not exceeding 4 to 5 cc per sec.) were calibrated by the method of displacement of water from a graduated vessel. With all flowmeters of larger capacity a wet test meter was employed. Because of the comparatively high solubility of acetylene in water, neither of the foregoing methods of calibration was applicable to this gas. Therefore, a system was devised by which a volume of acetylene could be withdrawn from the tank, measured, and then displaced under constant pressure through the flowmeter by water that was maintained saturated with acetylene gas.

In all calibrations the pressure at the exit of the flowmeter was atmospheric. During the experiments the exit pressure generally rose a few mm Hg above atmospheric pressure because of the flow resistance of the mixing chamber and the burner tube, and corrections became necessary to reduce the flowmeter readings to volumes delivered at the burner port. Theoretically, if the flow through the meter follows Poiseuille's law, the volume passing through the capillary per unit time at a given scale reading is independent of pressure; hence, the volume delivered at the port is increased by the factor $(1+\Delta P/P_{at})$, where ΔP is the excess of pressure above atmospheric at the flowmeter exit and P_{at} is the prevailing atmospheric pressure. If the constriction of the flowmeter consists of a plate orifice, the volume passing through the orifice per unit time at a given scale reading is proportional to the inverse of the square root of the pressure at the meter entrance (see, for example, Whitwell[9]) and hence, the volume delivered at the port is increased approximately by the factor $(1+\Delta P/P_{at})^{\frac{1}{2}} \simeq 1+\frac{1}{2}\Delta P/P_{at}$. Tests have shown that, for the square-cut capillaries used in this work, the correction factor could be written as $1+y\Delta P/P_{at}$, where for air, oxygen, and acetylene, $y=0.5$, and for hydrogen, $y=0.8$.

Pyrex-burner tubes were used for the series of experiments with hydrogen-air mixtures. For mixtures of hydrogen and oxygen, tubes of

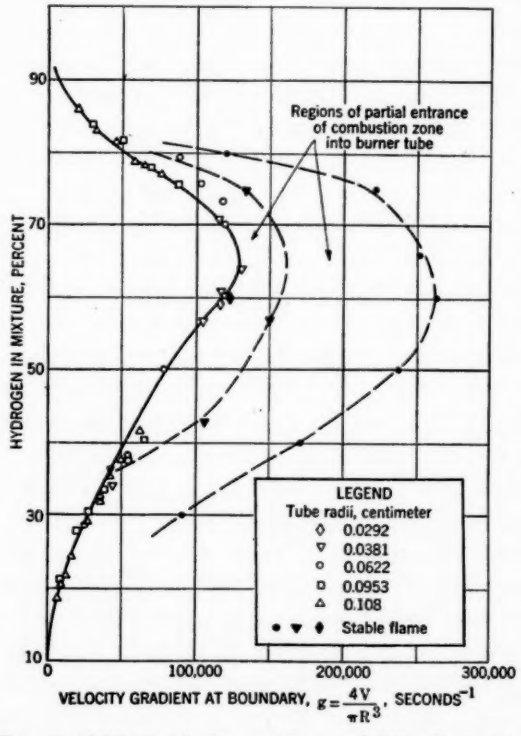

FIG. 8. Critical velocity gradients at boundary of gas stream for flashback of hydrogen-oxygen flames in cylindrical water-cooled tubes of different diameters.

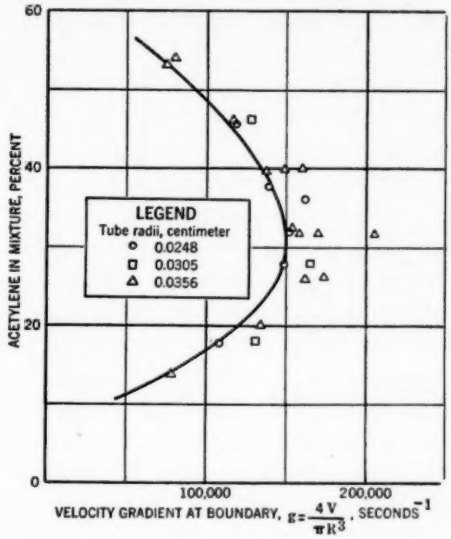

FIG. 9. Critical velocity gradients at boundary of gas stream for flashback of acetylene-oxygen flames in cylindrical water-cooled tubes of different diameters.

[9] J. C. Whitwell, Ind. Eng. Chem. **30**, 1157 (1938).

Pyrex and a porcelain thermocouple tube with an inside diameter of 0.058_4 cm were used. The burner tubes for acetylene-oxygen flames were made by drilling holes of 0.049 to 0.071 cm diameter in brass rods. To provide for laminar gas flow at the orifice, the length of any burner tube was at least 40 times its inner diameter.

Determinations of limits of inflammability between plane parallel plates for natural gas-air mixtures of 6.0 to 11.5 percent natural gas were made with the use of a rectangular metal burner whose cross section was of 1.6-cm length and of adjustable width. The limiting width for the downward propagation of a given mixture was measured with a micrometer. Inflammability limits were redetermined in a cylindrical tube of known diameter and compared with older data to preclude errors arising from possible changes in natural gas composition.

The pressures developed in the acetylene-oxygen flames were measured by a water barometer, which, at one side, was attached to the burner tube just below the orifice, and open to the atmosphere at the other side. A continuous flow of water through the jacket surrounding the burner tip was required in order to obtain constant values.

(B) Ranges of Flashback and Flame Tilt

From the values of the flow rates at which instantaneous—or true—flashback of hydrogen-air and hydrogen-oxygen flames occurred, the velocity gradients at the wall may be calculated. Plots of the critical velocity gradient *versus* mixture composition for these two types of flames (solid curves, Figs. 7 and 8) show the behavior expected theoretically, that is, the velocity gradient for flashback of a flame of a given mixture composition is independent of the tube diameter. However, the foregoing flashback data lose their practical significance because the regions of tilted flame, shown by the areas between the dotted and solid curves of Figs. 7 and 8, become much more extensive than is the case with natural gas-air flames. Actually these regions constitute a continuation of the range of unstable flame, inasmuch as the development of a tilted flame is followed invariably by flashback except for very lean or rich mixtures.

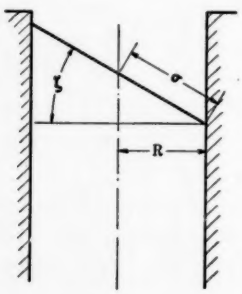

FIG. 10. Idealized combustion zone of tilted flame.

TABLE I. Calculation of K at the limit of the tilted flame range for various gas mixtures.

R cm	g sec.$^{-1}$	$K\times10^{-3}$, sec.$^{-1}$
9 percent natural gas+91 percent air; $S_u=38$ cm/sec.		
0.775	652	0.78
0.709	504	0.67
0.649	493	0.68
0.534	494	0.65
0.440	433	0.96
34 percent hydrogen+66 percent air; $S_u=230$ cm/sec.		
0.226	18,100	21
0.147	14,600	19
0.108	13,500	22
60 percent hydrogen+40 percent oxygen; $S_u=790$ cm/sec.		
0.0622	265,000	300
0.0381	158,000	230
0.0292	122,000	360

Flashback induced by flame tilt, as distinguished from the instantaneous phenomenon, is rather easily recognized with hydrogen flames. While hydrogen-air flames are not distinctly visible because of their low luminosity, the existence of tilt, though short-lived, can be observed in a shadow picture of the flame; with hydrogen-oxygen flames, the brilliance and pinpoint smallness of the cone often obscures the partial entrance of the flame into the tube, but a time-lag is observed between the formation of a flame and flashback. Rich flames of acetylene-oxygen mixtures may be drawn into the tube at several places around the rim, thus giving rise to a pronged flame which sometimes rotates because the points of entry of the flame shift from time to time. Since, as discussed below, the process of ignition induces flashback in acetylene-oxygen mixtures at flows considerably exceeding the true flashback limit, these mixtures were first ignited at flows far within the stable flame range, and the flow was then reduced until flashback occurred. In this process the flame

became strongly tilted and tended to flash back on slight disturbances; therefore, the flashback limits shown in Fig. 9 probably represent the lowest obtainable limits induced by tilted flames, and the region of true flashback cannot be outlined exactly.

On the whole, the partial entrance of the combustion zone into the burner tube is a more complicated phenomenon in acetylene-oxygen flames than in other flames. The limits of the tilted flame range could not be reproducibly established. They seemed to depend largely on fortuitous changes in the contour of the burner port. The intense heat and the radial gas flow at the flame base (cf. Fig. 5) melted away the original sharp edge of the tube and formed an irregular recess around the port.

Since tilted flames are formed by partial flashback, it appears that, above some limiting value of the gradient g of gas velocity at the tube wall, tilted flames cannot be formed. However, this limiting value changes with tube diameter, since the phenomenon depends on the deflection of the flow lines, that is, the pressure that the combustion zone exerts normal to the tube axis. If the combustion zone is assumed to be a plane surface within the burner tube, as shown in Fig. 10, the component of pressure normal to the tube axis may be taken proportional to the sine of the angle ζ; and, at the limit of the tilted flame range, the ratio $g/\sin\zeta$ may be expected to remain the same for a given mixture composition in tubes of different diameters. From geometrical relations

$$\sin\zeta=\left(1-\frac{R^2}{\sigma^2}\right)^{\frac{1}{2}}=\left(1+\frac{R}{\sigma}\right)^{\frac{1}{2}}\cdot\left(1-\frac{R}{\sigma}\right)^{\frac{1}{2}}, \quad (3)$$

where σ is the major semi-axis of the elliptical combustion zone of area $\pi\sigma R$. Since the ratio R/σ is of a magnitude comparable to 1, Eq. (3) becomes approximately

$$\sin\zeta=1.4\left(1-\frac{R}{\sigma}\right)^{\frac{1}{2}}. \quad (4)$$

Equating the gas flow V with the gas flow through

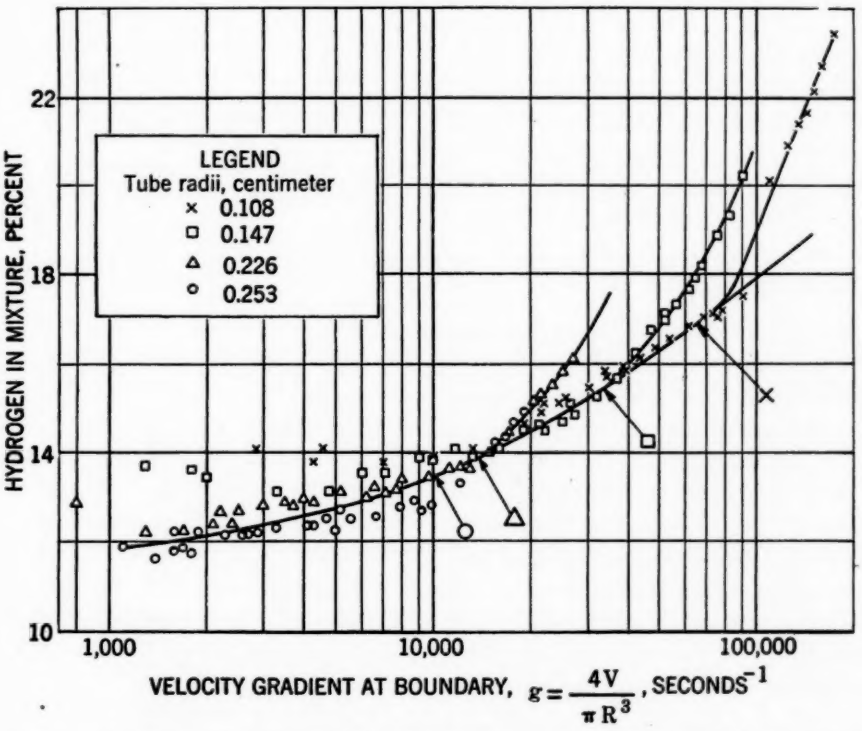

FIG. 11. Critical velocity gradients at boundary of gas stream for blow-off of hydrogen-air flames in cylindrical water-cooled tubes of different diameters. Arrows with symbols mark the beginning of turbulent flow (Reynold's number 2200) in the tubes corresponding to the symbols.

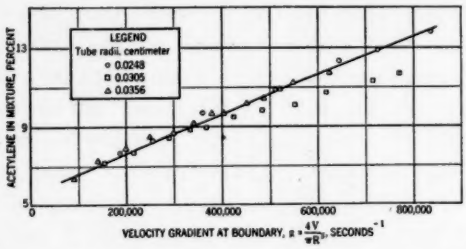

FIG. 12. Critical velocity gradients at boundary of gas stream for blow-off of acetylene-oxygen flames in cylindrical water-cooled tubes of different diameters.

the combustion zone

$$V = \pi\sigma R S_u, \tag{5}$$

where S_u is taken to be constant over the zone. Substituting Eq. (1) in (5) and transforming

$$R/\sigma = 4S_u/gR, \tag{6}$$

and the condition that, at the limit of the tilted flame range, $g/\sin\zeta$ remains constant, may be written

$$\frac{g}{(1-4S_u/gR)^{\frac{1}{2}}} = K. \tag{7}$$

Table I contains numerical values of K for the various gas mixtures investigated. The data for natural gas-air mixtures are taken from Lewis and von Elbe.[4,10] The burning velocities for hydrogen mixtures are taken from Jahn.[7] The constancy of the K values is satisfactory.

(C) Range of Blow-off

Figures 11 and 12 show the critical velocity gradients for blow-off of hydrogen-air and acetylene-oxygen flames. The hydrogen-oxygen flames have not been investigated because their blow-off curves generally fall outside the laminar flow range. This is also largely true for hydrogen-air flames. Since Eq. (1) for the velocity gradient is valid only for laminar flow, the extension of this equation to the range of turbulent flow yields values of g of obscure physical significance that form curves branching off the main laminar flow curve. By combining Eq. (1) with the equation for the Reynolds number,

$$2\rho V/\pi\eta R = 2200, \tag{8}$$

the gradient g_t at the point of transition from laminar to turbulent flow is found to be

$$g_t = 2\eta(2200)/R^2\rho. \tag{9}$$

It is seen that each curve of Fig. 11 undergoes a pronounced change in slope at the value of g_t (indicated by arrows in the figure), computed for the corresponding tube.

Figure 11 also shows that the critical velocity gradients for blow-off become dependent on the tube diameter when the diameter and the gas flow are very small. Under these conditions the quenching effect of the port rim penetrates into the interior of the stream beyond the linear range of the gas velocity curve; therefore, blow-off is attained with a smaller velocity gradient.

TABLE II. Pressure difference between unburned gas and atmosphere for acetylene-oxygen flames.

Acetylene in mixture percent	Total gas flow cc/sec.	Flame pressure cm H_2O	
Inside diameter of burner tube, 0.049 cm			
18.0	6.0	2.0	
28.0	6.0	5.2	
46.0	6.0	3.4	
Inside diameter of burner tube, 0.061 cm			
14.0	4.0	1.2	
	8.0	0.9	
	12.0	1.2	
			Av. 1.1
18.0	6.0	2.4	
	9.0	2.3	
	12.0	2.5	
			Av. 2.4
23.0	6.0	3.4	
	9.0	3.4	
	12.0	3.6	
			Av. 3.5
28.0	8.0	5.0	
	10.0	5.3	
	11.0	5.4	
	12.0	5.2	
	14.0	5.7	
			Av. 5.3
36.0	6.0	5.6	
	9.0	5.4	
	12.0	5.5	
			Av. 5.5
46.0	6.0	3.4	
	8.0	3.3	
	10.0	3.7	
			Av. 3.5
52.0	4.0	1.3	
	5.0	1.5	
	6.0	1.5	
	8.0	1.7	
			Av. 1.5

[10] The apparent anomalous extrusion of the g_F curve for a tube of 1.550-cm diameter (cf. reference 4, Figs. 8a and 11) has been recognized to belong to the tilted-flame range.

TABLE III. Calculated temperatures and density ratios for acetylene-oxygen flames of various mixture compositions. ($T_u = 291°K$, $P = 1$ atmos.)

C_2H_2 in mixture, percent	Mole fraction of reaction products at equilibrium								T_b (°K)	$\frac{\rho_u}{\rho_b}$
	CO	CO_2	O_2	O	OH	H_2O	H_2	H		
14.0	0.084	0.183	0.471	0.075	0.098	0.074	0.005	0.011	2980	10.75
28.6	0.326	0.118	0.099	0.113	0.144	0.078	0.026	0.090	3303	14.61
35.7	0.441	0.076	0.028	0.076	0.118	0.073	0.057	0.127	3366	15.95
45.5	0.556	0.021	—	0.021	0.035	0.035	0.135	0.198	3357	18.13
50.0	0.600	—	—	—	—	—	0.206	0.194	3288	18.83

An equivalent statement is that, for a given velocity gradient, flames of richer mixtures can be blown off in small tubes. This is illustrated by the lower part of Fig. 11, where the critical gradients for blow-off in small tubes lie above those determined in larger tubes.

(D) Flame Pressure and Burning Velocity

The pressure difference on both sides of the combustion zone that is caused by the mass acceleration within the zone is given by the equation[5] (cf. Lewis and von Elbe):[11]

$$p_u - p_b = \Delta p = \rho_u S_u^2 (\rho u/\rho_b - 1). \qquad (10)$$

The pressure p_u represents essentially the pressure throughout the whole stream of unburned gas because the pressure gradient along the burner tube is very small; p_b is substantially identical with the pressure of the surrounding atmosphere, so that Δp may be taken as the pressure difference between the gas in the burner tube and the outer atmosphere.

For natural gas-air mixtures the flame pressure Δp, calculated from values of S_u and ρ_u/ρ_b,[4] is only 0.01 cm of water for the strongest mixture; on the other hand, for acetylene-oxygen mixtures, pressures up to 5.5 cm of water are observed. This is shown in Table II. The resulting compression of an acetylene-oxygen mixture in the burner and connecting tubes at the instant of ignition slows down the gas stream momentarily to such an extent that flashback occurs over a considerable range of gas flows that would otherwise yield stable flames. In determining the flashback point, it is therefore necessary to ignite the mixture at a much higher flow, and to reduce the flow gradually until flashback occurs.

[11] B. Lewis and G. von Elbe, *Combustion, Flames, and Explosions of Gases* (Cambridge University Press, 1938), pp. 202–3.

Since the pressures of acetylene-oxygen flames can be measured conveniently and rather accurately, they may be used to calculate the burning velocities. For this purpose, ρ_u/ρ_b is calculated from the equation:

$$\rho_u/\rho_b = \frac{\Sigma m_b}{\Sigma m_u} \cdot \frac{T_b}{T_u}, \qquad (11)$$

where Σm is the total number of moles and T the absolute temperature. No correction is required for the small pressure difference between burned and unburned gas. Values of $\Sigma m_b/\Sigma m_u$ and T_b,

TABLE IV. Inner cone dimensions and burning velocities calculated from cone areas of acetylene-oxygen flames.

Acetylene in mixture percent	Total gas flow cc/sec.	Cone base, mm	Cone height, mm	Cone area mm^2	Burning velocity (S_u) cc/sec.
Inside diameter of burner tube, 0.049 cm					
18.0	6.0	0.858	1.330	1.89	318
	8.0	0.779	1.759	2.21	363
	10.0	0.771	2.083	2.57	389
28.0	6.0	0.761	1.112	1.41	427
	8.0	0.731	1.374	1.63	490
	10.0	0.717	1.697	1.96	515
36.0	6.0	0.782	1.149	1.49	402
	8.0	0.873	1.461	2.09	383
	10.0	0.784	1.737	2.19	456
Inside diameter of burner tube, 0.071 cm					
14.0	12.0	0.959	1.954	3.03	396
	16.0	0.985	2.550	4.02	398
18.0	9.0	0.859	1.288	1.83	491
	12.0	0.945	1.588	2.46	488
	15.0	0.905	2.006	2.92	514
23.0	12.0	1.015	1.362	2.32	518
	15.0	1.022	1.771	2.96	507
	18.0	1.078	2.090	3.70	493
36.0	15.0	1.041	1.650	2.83	530
	20.0	1.028	2.112	3.51	570
46.0	12.0	1.192	1.650	3.29	365
	15.0	1.116	1.999	3.64	384
52.0	10.0	1.080	1.815	3.21	312
	13.0	1.131	2.210	4.05	321

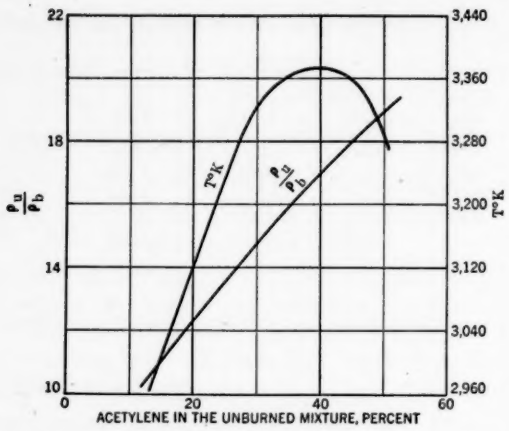

FIG. 13. Ratio of densities, ρ_u and ρ_b, of unburned and burned gas and absolute temperature of acetylene-oxygen flames. Initial temperature 291°K, pressure = 1 atmos.

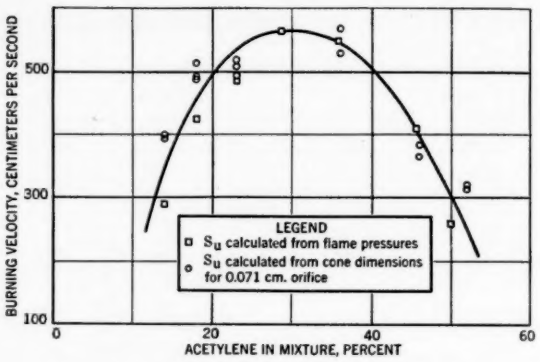

FIG. 14. Burning velocity curve for acetylene-oxygen mixtures.

for $T_u = 291°K$ and atmospheric pressure, are calculated thermodynamically, as described elsewhere,[12] with all possible dissociation equilibria considered. The results are summarized in Table III and Fig. 13. For mixtures of 50 percent to 28.6 percent acetylene, the calculations are given by Montagne.[13] Since these calculations do not extend to leaner mixtures, the calculation for the 14 percent mixture is added.

The usual method of determining burning velocities, as originally proposed by Gouy, consists in measuring the area F of the inner cone and the gas flow V; taking the gas flow normal to the combustion zone as $S_u \times F$, one obtains

$$S_u = V/F, \tag{12}$$

where S_u represents an average value from tip to base. It is hardly worth while to determine the cone area precisely; instead, F may be calculated from the cone height h and the radius R' of the base by the equation for the right circular cone

$$F = \pi R'(R'^2 + h^2)^{\frac{1}{2}}. \tag{13}$$

Table IV contains values of $2R'$ and h, measured by means of a cathetometer, for various acetylene-oxygen flames. It may be noted that in flames of this type the diameter of the cone base considerably exceeds the tube diameter. Constant values are obtained with a burner tube of 0.071-cm diameter, while in the smaller tube of 0.049-cm diameter, the gas flow appreciably affects the results, indicating a considerable influence of the port rim. Figure 14 shows the values of S_u obtained from flame pressures and cone dimensions, respectively; although the two methods are profoundly different, the results agree very well with each other.

[12] Reference 11, pp. 285–93.
[13] M. P. Montagne, Chaleur et Industrie **19**, 54 (1938).